AD-A135 663 HOLOGRAPHIC FLI (FRING LINEARIZATION INTERFEROMETRY) 1/1
FOR DETECTION OF EE.. (U) HONEYWELL ELECTRO-OPTICS DIV
LEXINGTON MA G O REYNOLDS ET AL. 08 OCT 83 8309-38
UNCLASSIFIED AFOSR-TR-83-1058 F49620-82-C-0001 F/G 14/5 NL

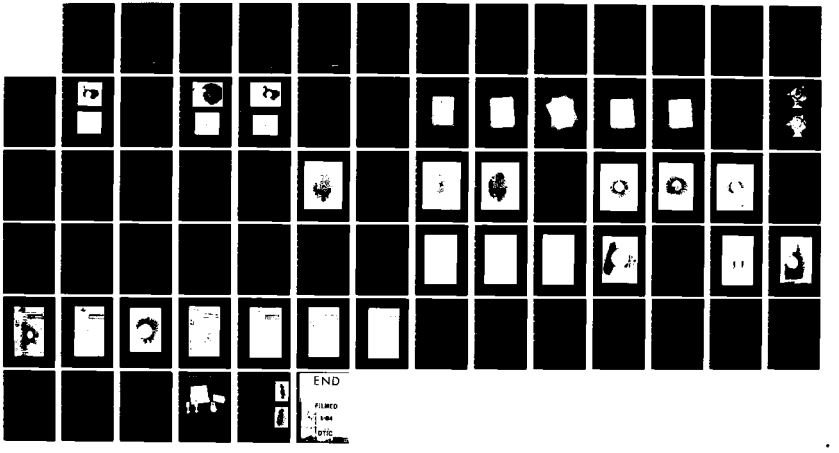

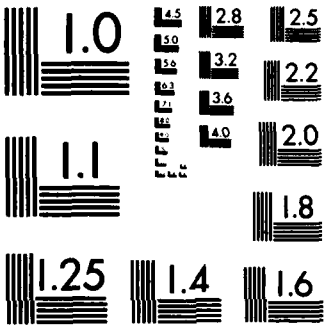

AFOSR-TR- 83-1058

8309-38

HOLOGRAPHIC FLI FOR DETECTION OF DEFECTS

Interim Report

8 October 1983

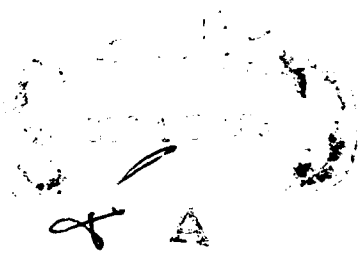

Honeywell

8309-38

HOLOGRAPHIC FLI FOR DETECTION OF DEFECTS

Interim Report

January 15, 1983 to August 15, 1983

Honeywell

ELECTRO-OPTICS DIVISION
2 Forbes Road
Lexington, MA 02173

UNCLASSIFIED

SECURITY CLASSIFICATION OF THIS PAGE (When Data Entered)

REPORT DOCUMENTATION PAGE	READ INSTRUCTIONS BEFORE COMPLETING FORM
1. REPORT NUMBER: AFOSR-TR- 83-1058	2. GOVT ACCESSION NO.: AD-A135663
3. RECIPIENT'S CATALOG NUMBER:	
4. TITLE (and Subtitle): Holographic FLI for Detection of Defects	5. TYPE OF REPORT & PERIOD COVERED: Interim Jan. 15, 1983 – Aug. 15, 1983
6. PERFORMING ORG. REPORT NUMBER: 8309-38	
7. AUTHOR(s): George O. Reynolds, P.I., Donald A. Servaes, John B. DeVelis, Honeywell EOD; Daniel Peirce, Ronald Mayville, Peter Hilton, Arthur D. Little, Inc.	8. CONTRACT OR GRANT NUMBER(s): F49620-82-C-0001
9. PERFORMING ORGANIZATION NAME AND ADDRESS: HONEYWELL Electro-optics Div., 2 Forbes Rd. Lexington, MA 02173	10. PROGRAM ELEMENT, PROJECT, TASK AREA & WORK UNIT NUMBERS: 61102F 2306A2
11. CONTROLLING OFFICE NAME AND ADDRESS: AFOSR/NE BOLLING AFB, DC 20332	12. REPORT DATE: October 1983
	13. NUMBER OF PAGES: 72
14. MONITORING AGENCY NAME & ADDRESS (if different from Controlling Office)	15. SECURITY CLASS. (of this report): UNCLASSIFIED
	15a. DECLASSIFICATION/DOWNGRADING SCHEDULE: NA

16. DISTRIBUTION STATEMENT (of this Report)

Approved for public release;
distribution unlimited.

17. DISTRIBUTION STATEMENT (of the abstract entered in Block 20, if different from Report)

NA

18. SUPPLEMENTARY NOTES

None

19. KEY WORDS (Continue on reverse side if necessary and identify by block number)

Holographic Interferometry, Non-Destructive Evaluation, Lasers Moire Techniques, Finite Element Analyses

20. ABSTRACT (Continue on reverse side if necessary and identify by block number)

This interim report describes the work performed during the first half of Phase II on the Two Step Holographic Fringe Linearization Interferometry Study. The FLI process consists of deflecting the object beam between holographic exposures to create linear fringes and spatial filtering of the image reconstructed from the hologram about the linear fringe carrier frequency. This filtering is meant to discriminate between subsurface defects and random fringe noise. During this phase a loading limitation

DD FORM 1 JAN 73 1473 EDITION OF 1 NOV 65 IS OBSOLETE

UNCLASSIFIED

SECURITY CLASSIFICATION OF THIS PAGE (When Data Entered)

20.

for the FLI process (of one quarter wave/linear fringe period for the out-of-plane deformations) was demonstrated. To circumvent this limitation two modifications to the FLI process were investigated: Four-Exposure FLI - a Moire technique and Laser Pulse separation control with dynamic loading. With the former method Linear fringes have been recovered from the random noise in a simulated laboratory experiment. Experiments to demonstrate the fringe shifts at defect locations with differential loading are still in progress. Preliminary experiments performed on the NADC holographic system indicate that it should be adequate, albeit cumbersome, to demonstrate the Laser Pulse Control Method. The finite element analysis is predicting the experimental fringe patterns obtained with static loading and the modeling effort for the dynamic loading experiments is discussed. Plans for the work to be done during the remainder of Phase II are given.

TABLE OF CONTENTS

LIST OF APPENDICES

LIST OF ILLUSTRATIONS

LIST OF ILLUSTRATIONS (Continued)

LIST OF ILLUSTRATIONS (Continued)

SECTION 1
INTRODUCTION

1.1 PROGRESS

This report describes the progress during the first half of Phase II on Contract F49620-82-C-0001 entitled "Use of Holographic Fringe Linearization Interferometry (FLI) for Detection of Defects". The results obtained in this phase to date show that holographic FLI as orginally conceived has a severe loading constraint, to the point of being impractical. Two methods for overcoming this constraint, and hence preserving the data processing advantages of FLI, were conceived. These methods are laser pulse control with linear fringes and dynamic loading techniques, and four exposure (two-laser) FLI, a moire technique. Both alternate methods have been analyzed. Analysis of the moire method shows that the loading constraint can be significantly relaxed. In addition, experimental results show that linear fringes in the moire pattern are carried by the arbitrary surface deformation pattern (noise) in the holographic interferogram. The computer model has corroborated the accuracy of holographic interferometry for monitoring surface displacements and has predicted holographic signatures for cracks and flaws with static loading. The dynamic loading analysis has commenced and indicates a preliminary design for the dynamic loading experiments which appears reasonable.

While the progress to date on this program has been sporadic due to the experimental complexity of the FLI process, we are very encouraged with the present four exposure, (two-laser) moire technique. It appears experimentally feasible, should be desensitized in its response to the load, and retains the linear fringe; hence, preserving the image processing advantages of FLI. In addition, the finite element modeling effort has been extremely successful in predicting the holographic fringe patterns caused by out-of-plane surface deformation with static loading mechanisms.

In this report we first define the research objective and delineate the significant accomplishments to date. We then discuss the basic experiments which illustrate the loading limitation, (i.e., out-of-plane displacements must be less than one quarter wave/linear fringe period) which is imposed on conventional holographic FLI. We then discuss two methods for avoiding this loading limitation:

- pulse separation control, and
- four-exposure (two-laser) FLI - a moire technique.

The theoretical bases for both methods are given and the recovery of linear fringes by the moire method - a significant achievement - is demonstrated. Various configurations for implementing the moire method, in a practical manner, are described. The results of the finite element work are presented with good agreement between the ADL computer model and experimental results being demonstrated. This work is a very important foundation for the control of the various loading mechanisms which is anticipated later in the program. Plans for the work to be performed during the rest of Phase II are also outlined.

1.2 CONTRIBUTIONS TO THE REPORT

The principal investigator of this study is George O. Reynolds from the Honeywell Electro-Optics Division. Donald A. Servaes from Honeywell is the Project Experimentalist. John B. DeVelis, a consultant to Honeywell from Merrimack College, has contributed to the holographic portion of the study. Ronald A. Mayville, Peter D. Hilton and Daniel C. Peirce from Arthur D. Little, Inc. performed mechanical designs and system analysis under a subcontract.

SECTION 2
RESEARCH OBJECTIVE

The objective of the research in this program is to prove the concept of Holographic Fringe Linearization Interferometry (FLI) and determine its degree of utility. In the FLI technique, linear fringes are introduced in the formation step of double exposure holographic interferometry by utilizing a beam deflector in the object beam between the two holographic exposures. A subsequent spatial filtering operation is performed on the reconstructed image from the double exposure hologram. The filter is tuned to the frequency of the linear fringes. The purpose of the filter is to remove from the image the random fringes which commonly appear in double exposure holographic interferometry. These noise fringes occur due to the differential vibrations which exist in the test subject at the two different exposure times. The noise fringes are the prime cause of the difficulty in data interpretation of normal double exposure holograhic interferograms. The filtering step should remove the noise fringes and enhance the presence of shifts in the linear fringes due to subsurface defects. This enhancement is expected to simplify the process of locating the defects.

The prime goal of this research program is the experimental demonstration of the FLI technique for detecting and locating (not necessarily identifying or classifying) subsurface cracks and defects in various structures. Since FLI is potentially a large area inspection technique which is very compatible with image processing, its success can ultimately simplify the Nondestructive Evaluation (NDE) process for large military structures such as aircraft.

The experimental work to date has been performed by Honeywell EOD at the Advanced Concepts Group in Brighton, Massachusetts. Initial experimentation at NADC has also been performed. We anticipate performing more work at NADC during the remainder of the program. The modeling work and deformation analysis has been performed at Arthur D. Little, Inc. in Cambridge, MA.

SECTION 3
PROGRESS, PRELIMINARY RESULTS AND PLANS

The program is scheduled to be a three-phase study over a three-year period of time. This report discusses the work performed and the results obtained during the first half of Phase II.

The results to date indicate that the FLI technique must modified from that originally conceived in order to allow practical loadin echanisms to be utilized. Two modifications which preserve the data reductior vantages of FLI are currently being investigated:

- laser pulse control on double exposure holography with dynamic loading and
- moire methods using four exposure (two-laser) holography.

The initial experiments at NADC revealed that the first method may be difficult to demonstrate because of electronic control limitations on the current NADC holographic system. The moire method has been set up in Honeywell Labs and the preliminary results are indeed encouraging. Work is continuing in this vein to determine the effects of differential loading between exposures in the moire method.

The finite element analysis gives good qualitative agreement between theory and experiment for static loading conditions. The work on dynamic loading mechanisms has started with the result that the conditions for the initial experimentation appear practical.

During the remainder of Phase II we plan to demonstrate the feasibility of the Moire method with differential loading conditions (static) for specimens having various defects. The current model will be utilized to pre-

dict the limit of applicability of this method. Experimentation at NADC will be performed to determine the feasibility of realizing the pulse control method on their holographic system and work on the dynamic loading model will continue.

SECTION 4
TECHNICAL STATUS OF RESEARCH EFFORT

4.1 DOUBLE EXPOSURE EXPERIMENT

The annual report for Phase I showed that linear fringes could be recovered by filtering the image made in a triple exposure holographic arrangement. In this configuration the simulated noise was introduced during the third exposure, and subsequently removed in the filtering step. The first experiment performed during this phase of the project was to demonstrate the double exposure FLI configuration so that the experimentation could move to NADC system.

4.2 DOUBLE EXPOSURE TEST AND THE LOADING CONSTRAINT

In this experiment, a simple double exposure configuration was utilized to prove the feasibility of the holographic FLI concept. Three separate experiments were performed during this task.

4.2.1 Experiment #1

In the first double exposure holographic experiment an exposure of the plate was made. Between exposures, the plate was linearly tipped about the x-axis and the second holographic exposure was made. Reconstruction of this hologram resulted in linear fringes parallel to the x-axis whose frequency was directly proportional to the angle of the tip. The reconstructed image resulting from this experiment is shown in Figure 4-1a and its Fourier transform is shown in Figure 4-1b. Note that the direction of the diffraction due to the plate tip is vertical. The tip of the plate about the x-axis can be thought of as a simple type of out-of-plane deformation due to a load.

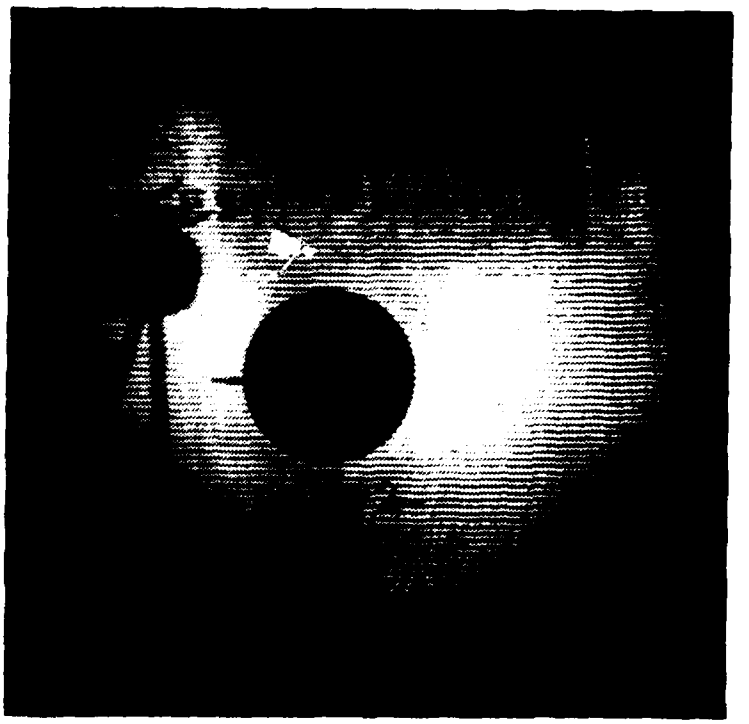

a. Reconstructed Image of Double Exposure Hologram Resulting from Tipping the Test Plate about the X-Axis between Exposures

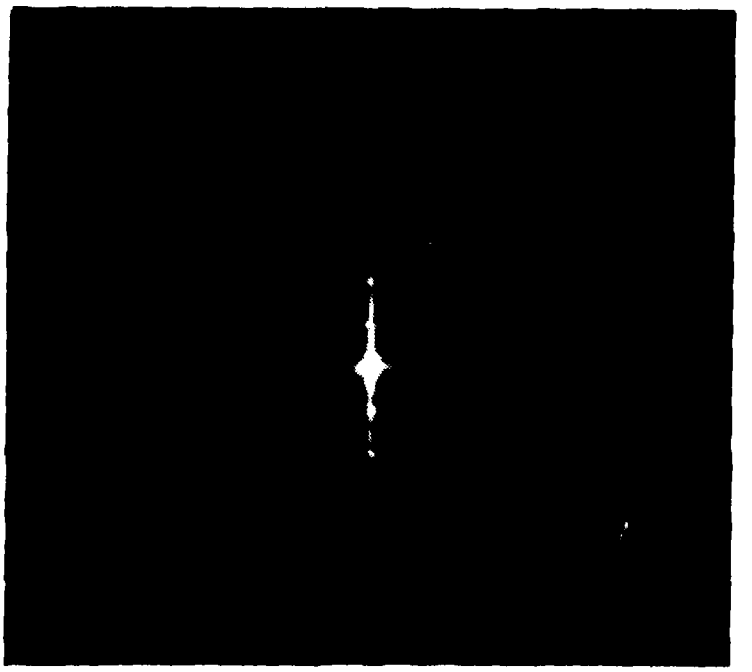

b. Fourier Transform Showing Delta Functions Along y-axis

Figure 4-1. Results of Experiment #1

4.2.2 Experiment #2

In the second double exposure holographic experiment the plate remained stationary and the object beam was rotated about the y-axis between holographic exposures. This motion corresponds to the introduction of the linear fringe. Reconstruction of the double exposure hologram resulted in linear fringes parallel to the y-axis as shown in Figure 4-2a. The resulting Fourier transform, as shown in Figure 4-2b, had diffraction spots oriented in the x-direction.

As expected, these two experiments show that the hologram is sensitive to the phase of the object beam independent of whether the phase change between exposures results from a motion of the surface or the tip in the object beam.

4.2.3 Experiment #3

The third experiment performed in this series combines the above two experiments and may be interpreted in the following manner. The first holographic exposure was made with the test plate parallel to the holographic exposure film plane. Between exposures, the object beam was rotated about the y-axis (this gives fringes localized on the object surface as discussed in the Phase I Annual Report) to create FLI linear fringes, and the plate was rotated about the x-axis to simulate a controlled loading applied to the test plate. The image resulting from this double exposure hologram and its Fourier transform is shown in Figure 4-3.

4.2.4 Discussion of Results

The behavior of the Fourier transform in Figure 4-3b indicates several limitations in the conventional holographic FLI concept. In order to remove random fringe noise in the optical filtering process of FLI, the carrier frequency of the linear fringes must stay close to the x-axis as shown in Figure 4-2b, so that light will pass through the spatial filter. However, Figure 4-3b shows that the position of the first order has rotated. This means

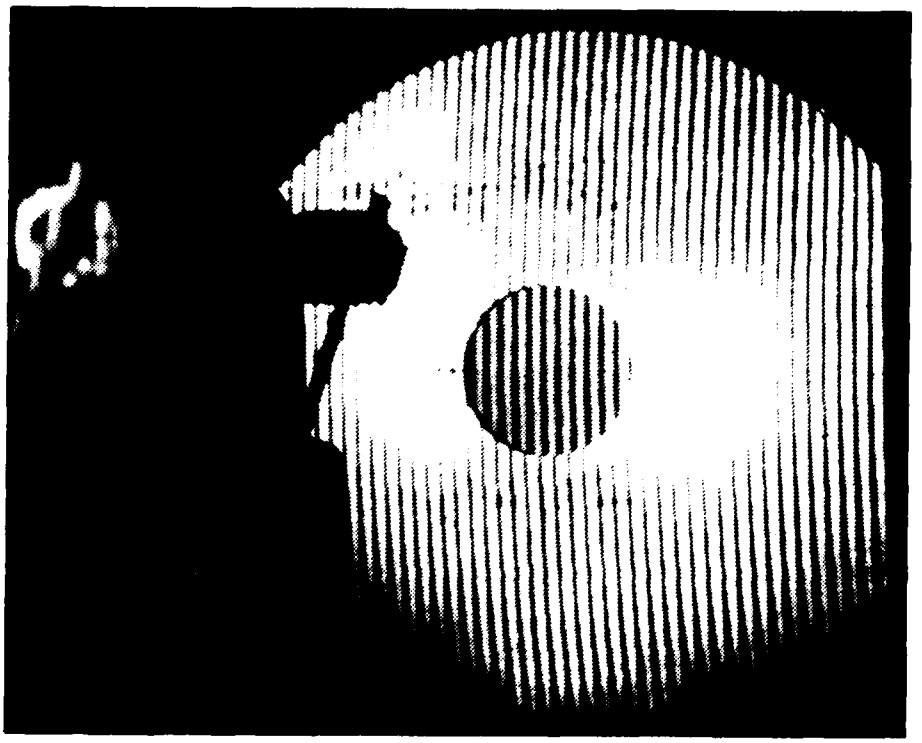

a. Reconstructed Image of Double Exposure Hologram Resulting from Rotating the Object Beam about the y-Axis between Exposures

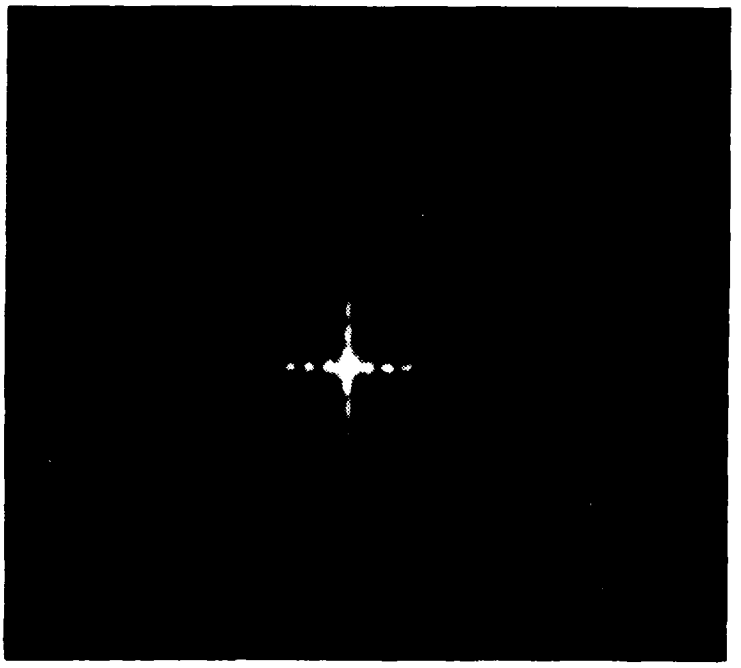

b. Fourier Transform Showing Delta Functions Along x-Axis Corresponding to the Linear Fringes

Figure 4-2. Results of Experiment #2

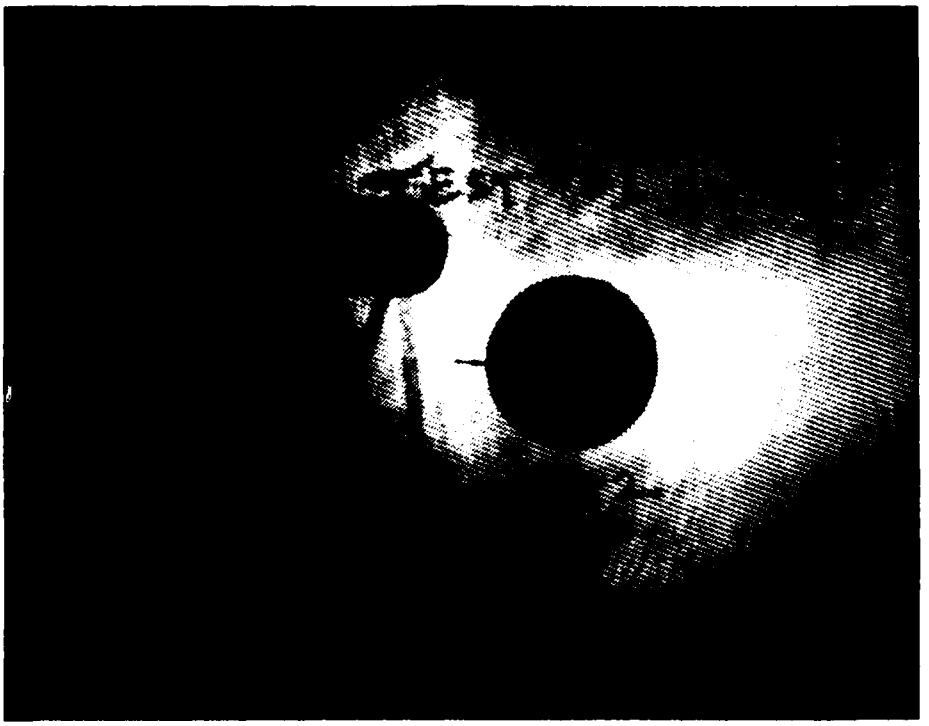

a. Reconstructed Image of Double Exposure Hologram Resulting from Rotating the Object Beam about the y-Axis and Tipping the Test Plate About the x-Axis Between Exposures

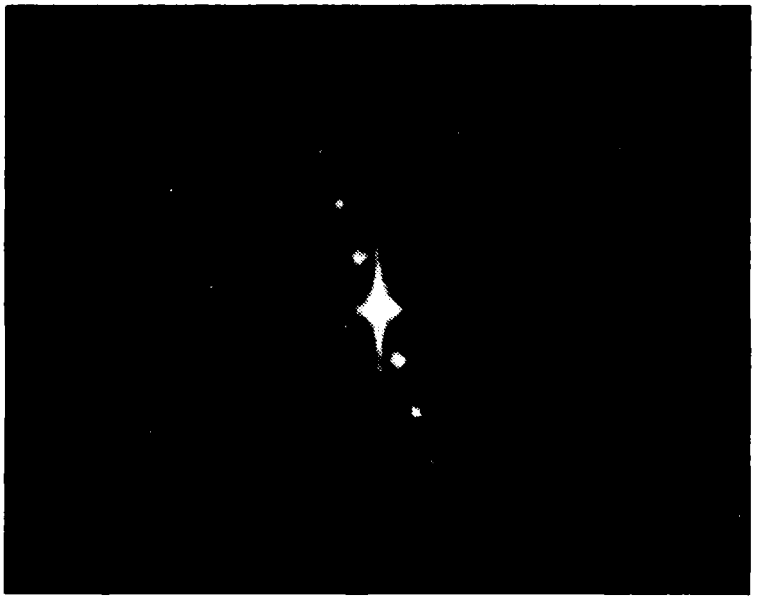

b. Fourier Transform Showing that the Delta Functions Rotate

Figure 4-3. Results of Experiment #3

that the position of the diffraction spot is dependent upon the vector addition of the phase due to the carrier frequency and phase due to the out-of-plane surface motion caused by the loading of the plate.

If the out-of-plane motion due to the differential loading between the holographic exposures is greater than one quarter wave/linear fringe period, then the vector addition of the phases will cause the position of the linear fringe frequency to randomly move and spread in transform space.

This renders the filtering step of the FLI ineffective. Thus, holographic FLI as originally conceived* will be extremely limited in its application due to this loading constraint because such loads will be extremely difficult to achieve in a practical manner.

Rather than pursue further experimentation with conventional FLI on the NADC system, the program emphasis was changed and methods for meeting the program goals within this loading constraint were investigated.

4.3 METHODS FOR CIRCUMVENTING THE LOADING CONSTRAINTS IN HOLOGRAPHIC FLI

Two approaches were formulated and investigated for overcoming this loading constraint. The first is to utilize moire holography, a desensitization method, and the second is to control both the time between pulses in double pulse holography and the dynamic loading mechanism to ensure that the surface does not move out-of-plane by more than one quarter wave/linear fringe period during the time between pulses. The investigations to date on these two modified approaches are discussed below.

4.3.1 Moire Methods for Desensitizing Holographic FLI

4.3.1.1 The Basic Moire Method: Periodic Functions

Moire fringes are observed when two periodic objects are superimposed and rotated with respect to each other[1,2,3]. The moire fringes occur because

---

* The original holographic FLI concept consisted of swinging the object beam between exposures to create a carrier frequency and perform subsequent optical spatial filtering about the carrier frequency to remove random fringe noise to ease the detection of defects in a subsequent image processing step.

the opaque part of one grating overlaps the transparent part of the other as seen in Figure 4-4. For gratings of equal period, d, superimposed at an angle θ, the period of the moire fringe is given by

$$D = \frac{d}{\theta} .$$

Thus, as the gratings rotate with respect to each other, the frequency of the moire fringes increase as seen in Figures 4-4b and 4-4c. If one of the gratings is kept stationary and the other one is moved in the x direction, the moire fringes move a distance D as the grating moves a distance equal to its period. These effects are illustrated in Figures 4d and 4e for a motion in the x direction of approximately d/2 and a fixed angle θ between the gratings to realize the moire fringe.

Mathematically, we may describe a moire fringe resulting from gratings of two different frequencies (note: the rotation in Figures 4b and 4c causes a frequency change of the grating projection along the x or y axis) as

$$I(x) = (1 + \cos \omega_1 x)[1 + \cos(\omega_2 x + \omega_3 y)] \tag{1}$$

$$I(x) = 1 + \cos \omega_1 x + \cos(\omega_2 x + \omega_3 y) + 1/2 \cos [(\omega_1 + \omega_2)x + \omega_3 y)]$$

$$+ 1/2 \cos [(\omega_i - \omega_2)x - \omega_3 y] \tag{2}$$

Since the moire fringe is sampled by the highest frequency grating, it must correspond to the difference frequency fringe in Eq. 2. This explains why the moire fringes in Figure 4-4 always have a lower frequency than the frequency of either grating. The sum frequency fringe is not seen because it is not properly sampled. Note: Eq. 2 shows that the moire fringes are superimposed on the two original gratings, i.e., the original gratings are still visible as seen in Figure 4-4. Also, the moire fringes make an angle to both original gratings since the rotated grating in Eq. 1 makes an angle, $\theta = \tan^{-1} (\omega_3/\omega_2)$

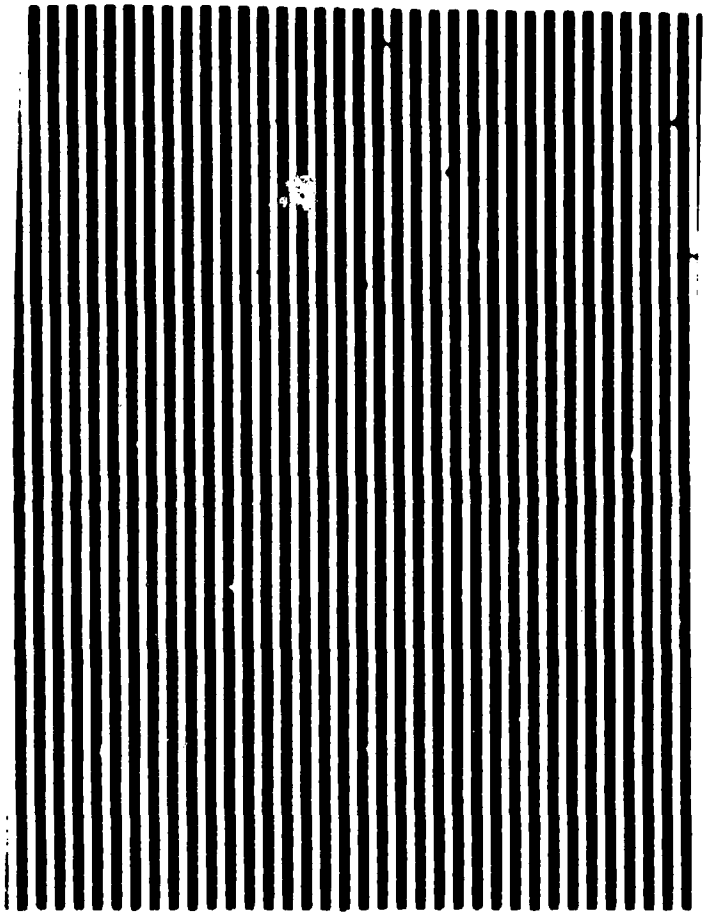

Figure 4-4a. Original Grating

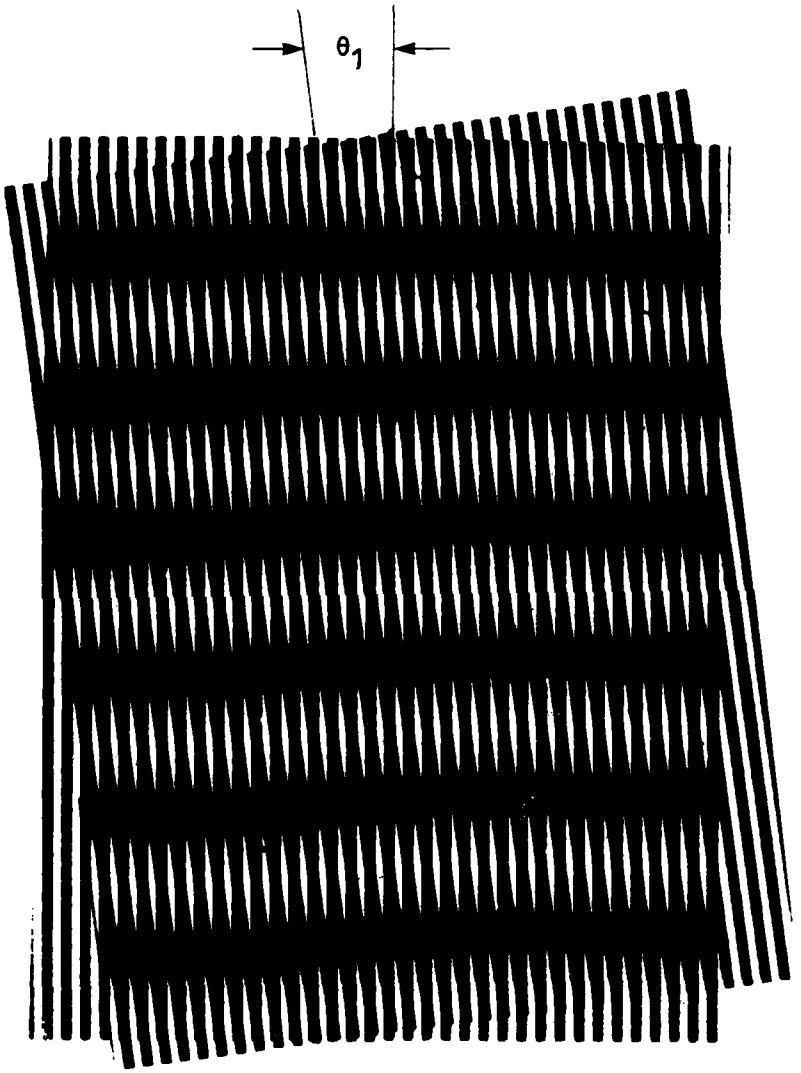

Figure 4-4b. Low Frequency Moire Resulting From a Rotation of One Grating Through an Angle, θ_1

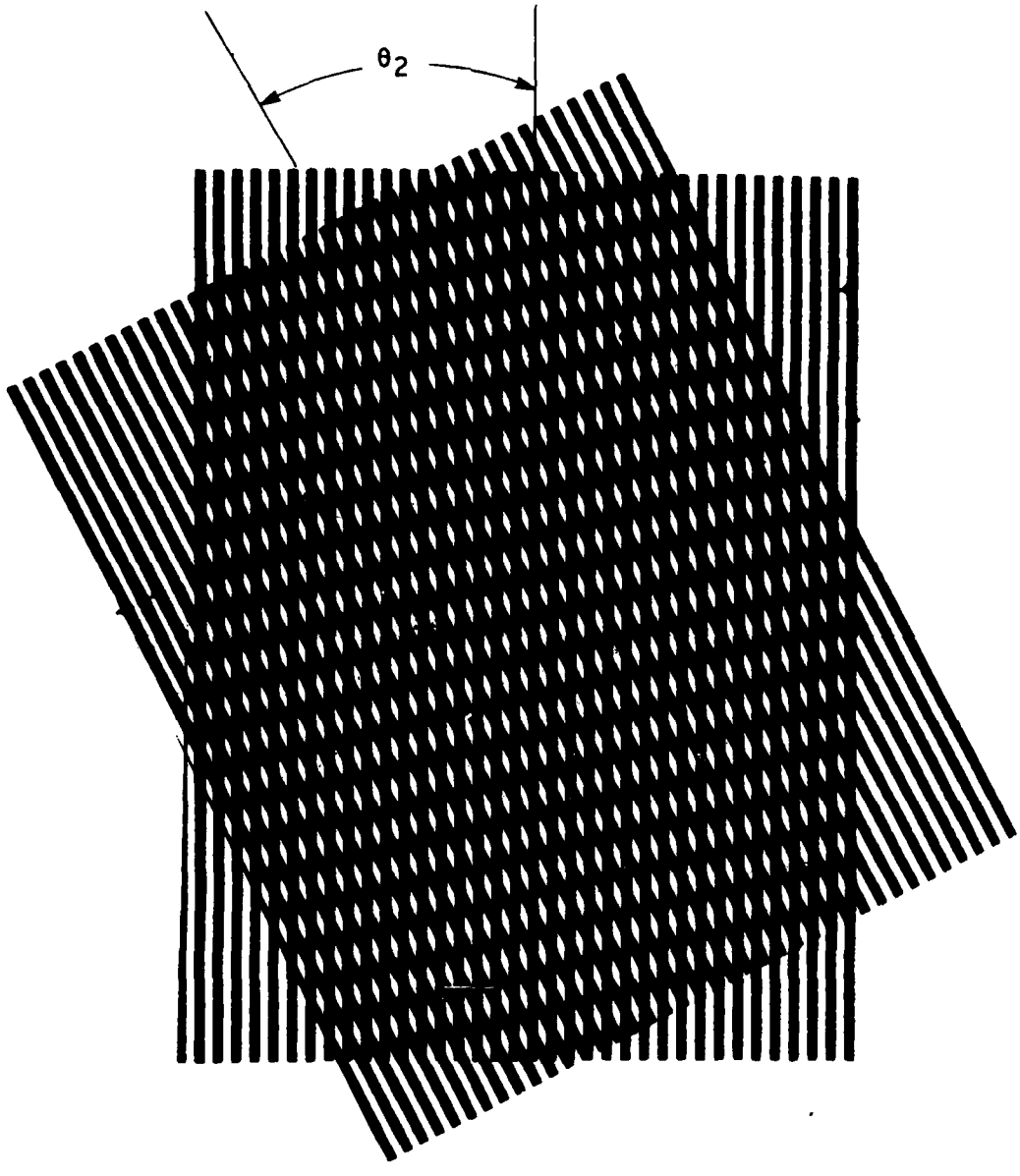

Figure 4-4c. High Frequency Moire Resulting From a Larger Rotation θ_2

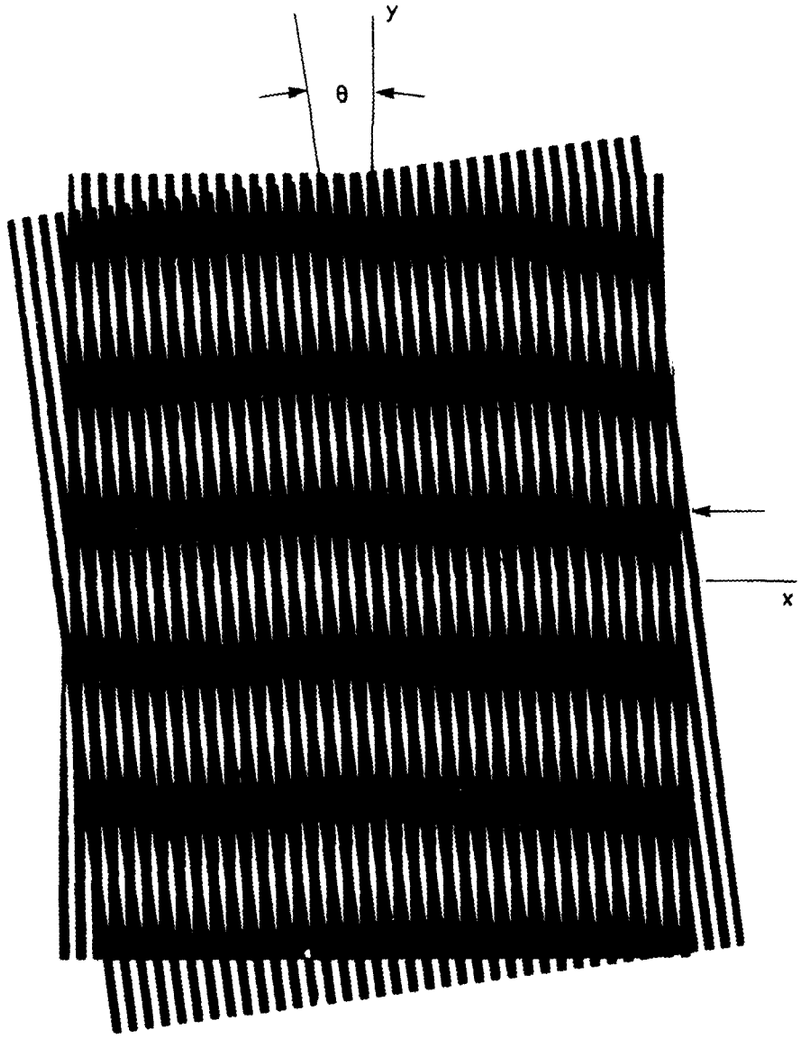

Figure 4-4d. Low Frequency Moire Resulting From a Fixed Angle, θ, Between the Gratings. Note Minimum of Moire Fringes at Position of Arrow Parallel to x-Axis

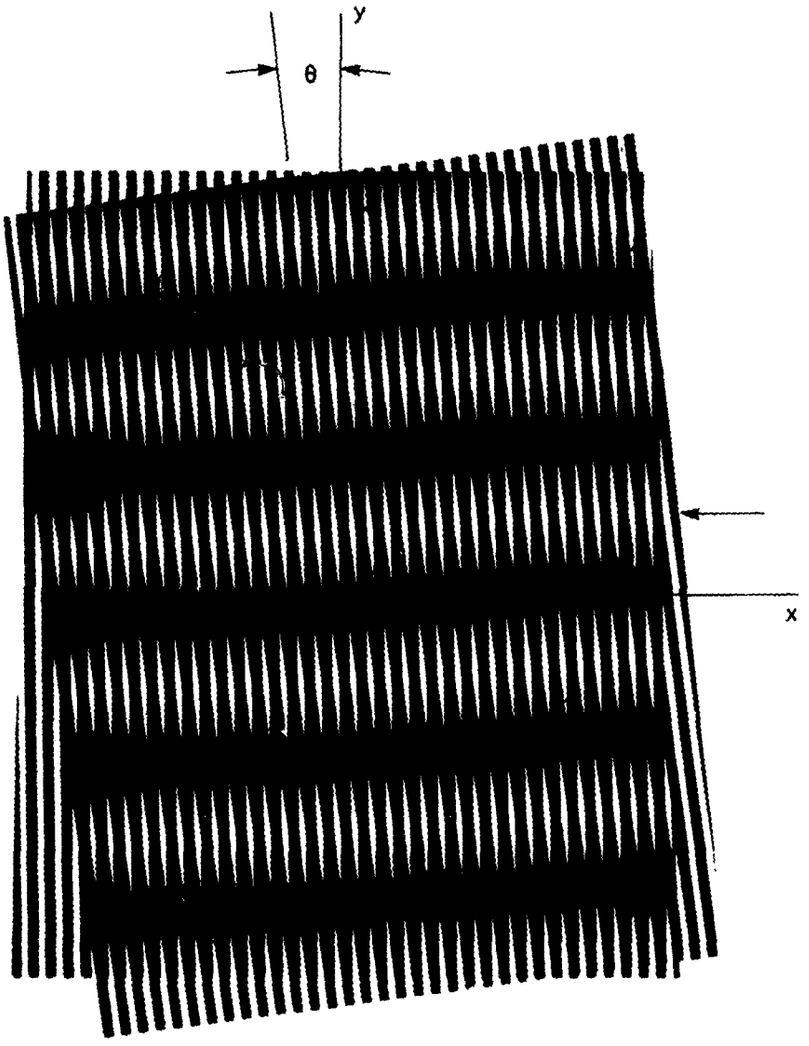

Figure 4-4e. Movement of Moire Fringe Position Resulting from Approximately One Half Period Displacement in the x-Direction. Notice that the Moire Fringe at the Position of the Arrow has Moved Approximately One Half Period.

8309-38

to the x axis. The moire fringe makes a large angle, $\theta' = \tan^{-1}[\omega_3/(\omega_1-\omega_2)]$ to the x axis. Note if $\omega_1 = \omega_2$, $\theta' = \pi/2$ and the moire fringes will be perpendicular to the x axis.

The moire technique has proven useful in many interferometric measurements for measuring displacements of surfaces[4]. The technique is often cumbersome because the object of interest has to be striped with a periodic function and measured with a reference grid.

4.3.1.2 Holographic Moire: Non-Periodic Functions

In holographic interferometry, moire-type effects have been introduced to desensitize the measurement accuracy of the techniques, using non-periodic carriers[3,5]. In this work multiple source, multiple index and multiple wavelength, effects have been utilized to create the moire effect. The desensitized capability of the two wavelength method is given by the factor $\Delta k = 2\pi\ (1/\lambda_1 - 1/\lambda_2)$ which results in a change in the contour interval of

$$\Delta I = \lambda_1\lambda_2/2\Delta\lambda. \qquad (3)$$

It is this moire desensitization method which we plan on utilizing to overcome the loading limitations of the holographic FLI process. In particular, we will extend the method described by Abramson[6] to achieve a desensitization with the FLI concept by utilizing moire methods.

4.3.1.3 The Abramson Experiment[6]

In this experiment a doubly-exposed hologram of a centrifugal pump was made. Between holographic exposures the internal pressure of the pump was changed, and a large rigid body motion, rotation, was also introduced to the pump. This rotation produced a great number of almost vertical straight fringes. The desired information concerning the pressure deformation is hidden by the unwanted vertical fringes on the reconstructed image as shown in Figure 4-5. The resulting moire fringe (difference fringes) represent the difference between the rigid body motion (i.e., rotation) and the rotation plus expansion due to pressure change as shown in Figure 4-6. Thus, the moire fringes show the deformation of the pump due to the pressure change between exposures.

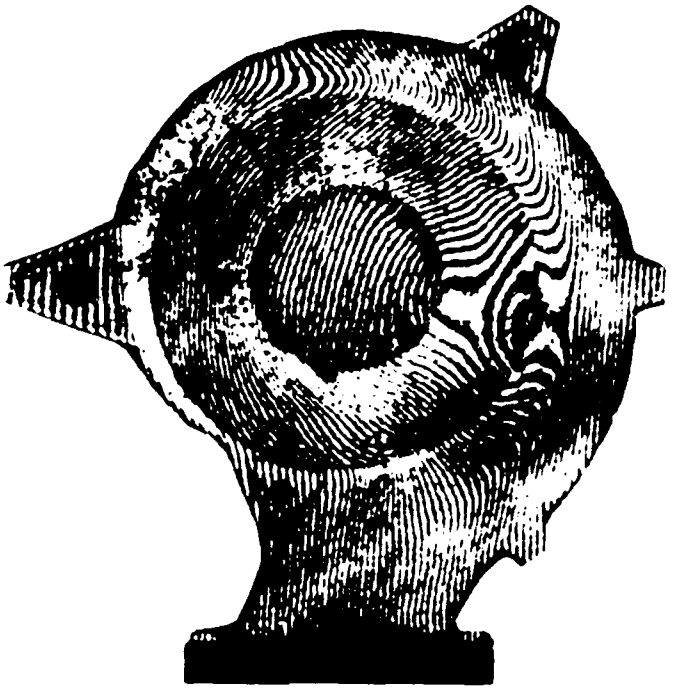

Figure 4-5. Reconstructed Image from a Doubly Exposed Hologram Made of a Centrifugal Pump with a Height of About 1 Meter. Between the Two Exposures the Internal Pressure of the Pump was Changed and the Pump was subjected to a Large Rigid Body Motion (i.e., Rotation) [after Abramson[6]]

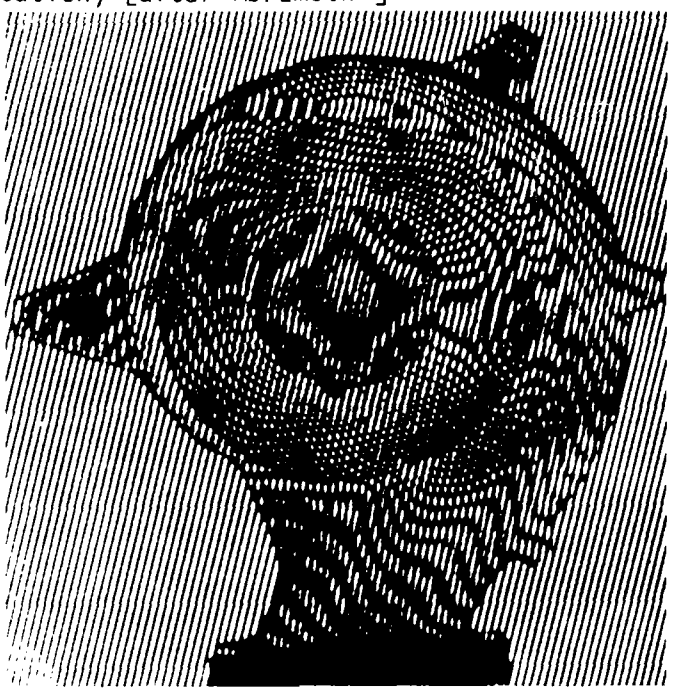

Figure 4-6. Moire Fringe of a Periodic Grating with Figure 4-5 Showing the Desensitized Reconstructed Image of Figure 4-5. Notice the Low Frequency (Moire) Fringes Not Present in Figure 4-5 which are Associated with the Out of Plane Deformation Due to the Pressure Change Given to the Pump Between Exposures. [after Abramson[6]]

Therefore, the moire technique, a desensitizing process, has been used to recover a small phase change in a hologram (deformation due to pressure) which was swamped by a large phase disturbance (rigid body motion).

Our suggestion for FLI is to invert this process, i.e., use the random fringe as a carrier and recover the linear fringe by the moire method. This linear fringe, which should carry the defect information when the test subject is properly loaded, can then be filtered and processed with automatic techniques to locate sub-surface defects.

4.3.1.4 Fringe Desensitization with Four Exposure (Two-Laser) FLI

Instead of moireing with a grating as done by Abramson[6] we propose using a four-exposure, two-layer, two hologram FLI process to recover the linear FLI fringes from the holographic moire of the random noise pattern produced by the dynamic loading. Experimentally, we propose using two pulsed lasers, (possibly different colors) as sources to illuminate the object. One of the lasers will have a beam swinging mirror in the object beam so that linear fringes can be introduced into one of the holograms by tilting the object beam between exposures. The initial pulses from the two lasers will occur simultaneously, and dynamic loading techniques will be used. This will ensure that both lasers (hence both holograms), see the same initial state of the surface. The second two pulses will be separated by a small time, δt, so that both double exposure holograms have essentially the same noise pattern. Photographing the reconstructed images fom the two holograms and moireing them will visualize the linear fringes (small phase) and the higher frequency defects such as subsurface cracks. Filtering of the moire fringes by the techniques described in the first year Annual Report[7] should result in high contrast FLI fringes showing the location of the defects as fringe shifts. The four-exposure, two-laser, two-hologram FLI process can probably be simplified by recording the holograms on the same film and obtaining the moire beats directly as suggested by Varner[8].

If the two lasers have different wavelengths, then the change in linear fringe frequency is given by $(k_1 - k_2)\,\alpha_0$ where

$$k_n = \frac{2\pi}{\lambda n} \; ; \; n = 1,2$$

and α_0 is the angle of the mirror which is tipped to introduce the linear fringes.

For example, if the two lasers are frequency doubled YAG (λ_1 = 0.53 μm) and Pulsed Ruby (λ_2 = 0.69 μm) then $\Delta\lambda/\lambda_1\lambda_2 = 0.3/\lambda_2$ so that the frequency of the linear fringe is 30% lower than it would be for double pulsed holography with a ruby laser. Thus, the moire fringes resulting from using two different lasers have a period characteristic of a laser with a longer wavelength. The mathematical analysis of this modified FLI process is given in Appendix A.

4.3.1.5 An Experimentation Scheme for Implementing Four-Exposure FLI

The following configuration (see Figure 4-7) for implementing the four-exposure FLI process has real time potential. This configuration reduces the photographic steps and automatically registers the reconstructed images for subsequent filtering and display of potential defects.

Consider the holographic recording system shown in Figure 4-7.

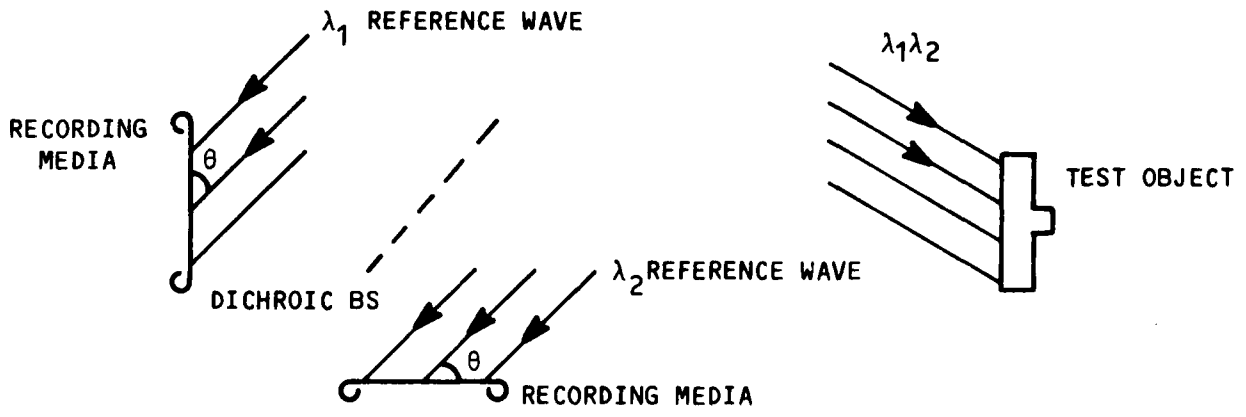

Figure 4-7. Schematic of Recording System for Four-Exposure FLI

The object is illuminated with light from two lasers and a common collimator. A mirror in one of the beams will be shifted between holographic exposures to create the linear fringes on one of the two double exposure holograms. The two films and the dichroic beam splitter (BS) make up a modified FLI sandwich which enables the construction of separate holograms simultaneously. In the ultimate application for NDE the two lasers must be initially synchronized to create simultaneous double pulses so that nanosecond pulses separated in time by a few microseconds can be realized. This will enable us to freeze the out-of-plane surface motions due to the vibrations created by dynamic loading. The two films in Figure 4-7 will then see nearly the same surface motions and defects in different colors. Also, we note that the recording media in Figure 4-7 can be the Honeywell Thermoplastic System or any other holographic real time recording media as well as film, dichromated gelatin, etc.

If the recording media (assume real time media) in Figure 4-7 are illuminated by the reference beam (or its conjugate) then two superimposed registered images of the object appear at the image plane in Figure 4-8. If we independently record these images on film or with another real time recording media, then the difference frequency of FLI will appear superimposed upon the noise field when moired with incoherent light. Note: If the two holograms are illuminated with two different lasers (e.g., λ_1, λ_2 as when they were made) then we avoid color aberrations and the image intensities from the two holograms will add independently. This gives a moire fringe of the form

$$\cos(\omega_1 x + \Delta k\ \Delta\phi) \qquad (4)$$

which is the desired output of the FLI process.

If coherent light from one laser is used to simultaneously reconstruct both holograms in Figure 4-8, then we get amplitude addition and squaring on the film in the image plane and the FLI effect (Eq. 4) will be realized as one of 16 terms as suggested by Varner.[8]

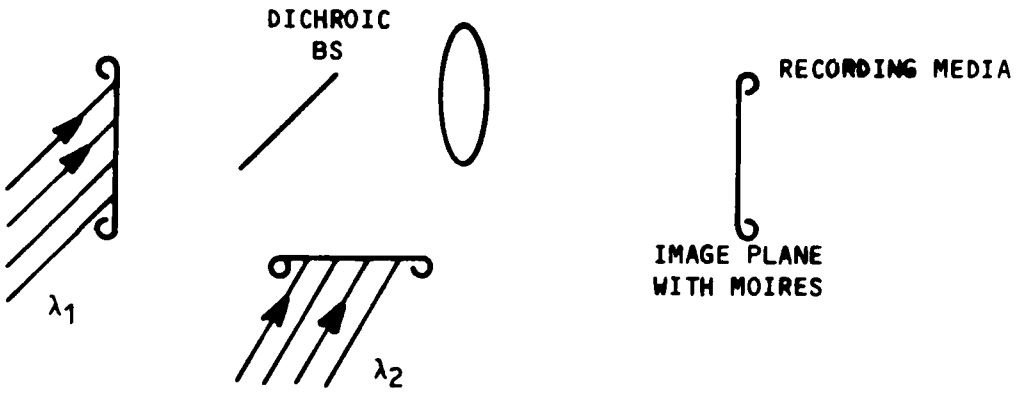

Figure 4-8. Schematic of Four-Exposure, Two-Color FLI Reconstruction System

Since the modified FLI from moire (Eq. 4) is superimposed upon the dynamic noise fringes, a subsequent spatial filtering operation on the output recording medium (e.g. ITEK PROM) can be performed to increase the contrast of the linear fringes. This is illustrated schematically in Figure 4-9. The filtered FLI output can then be analyzed in real time by a vidicon camera and image processing system to give the coordinates of the defect, (i.e., its location).

4.3.1.6 Experimental Demonstration of Four Exposure FLI Process

A simulation experiment was performed to demonstrate the feasibility of the four-exposure, two-laser FLI process. In this experiment, repeatable static forces were used so the two double exposure holograms could be made with the same laser at different times rather than using two lasers and dynamic forces. The experimental procedure was as follows:

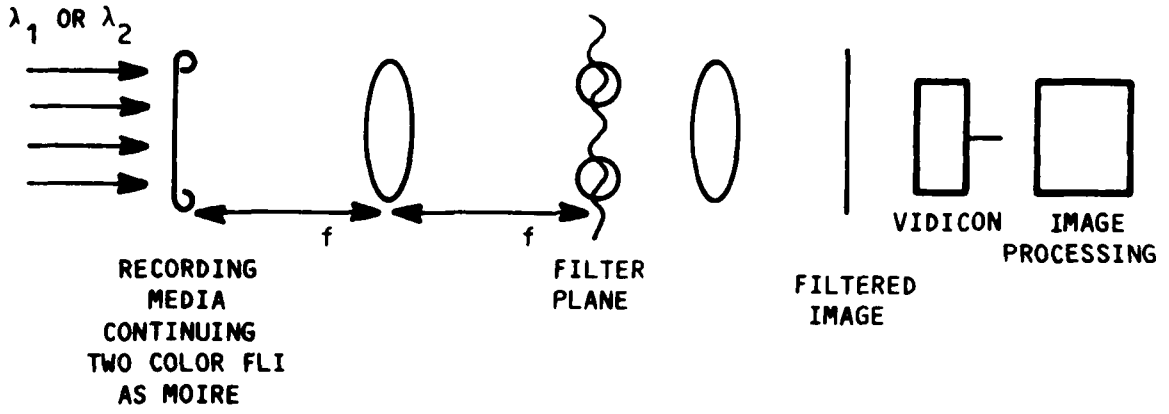

Figure 4-9. Schematic of Filtering System for Filtering Linear Fringes (Achieved by Moire Techniques) From Noise Background

1. The test body was hologrammed in state #1, its relaxed state. This is hologram #1.

2. The second exposure on hologram #1 was made after stressing the object by turning two thumb screws in the test fixture. This is state #2 of the object. This double exposure hologram was then processed and its reconstructed image (interferogram) subsequently photographed. This holographic interferogram is shown in Figure 4-10.

3. Another Double Exposure hologram is made. The first exposure on hologram #2 is the same as the second exposure on hologram #1. i.e. a hologram of the surface in state #2. The same laser can be used as for hologram #1.

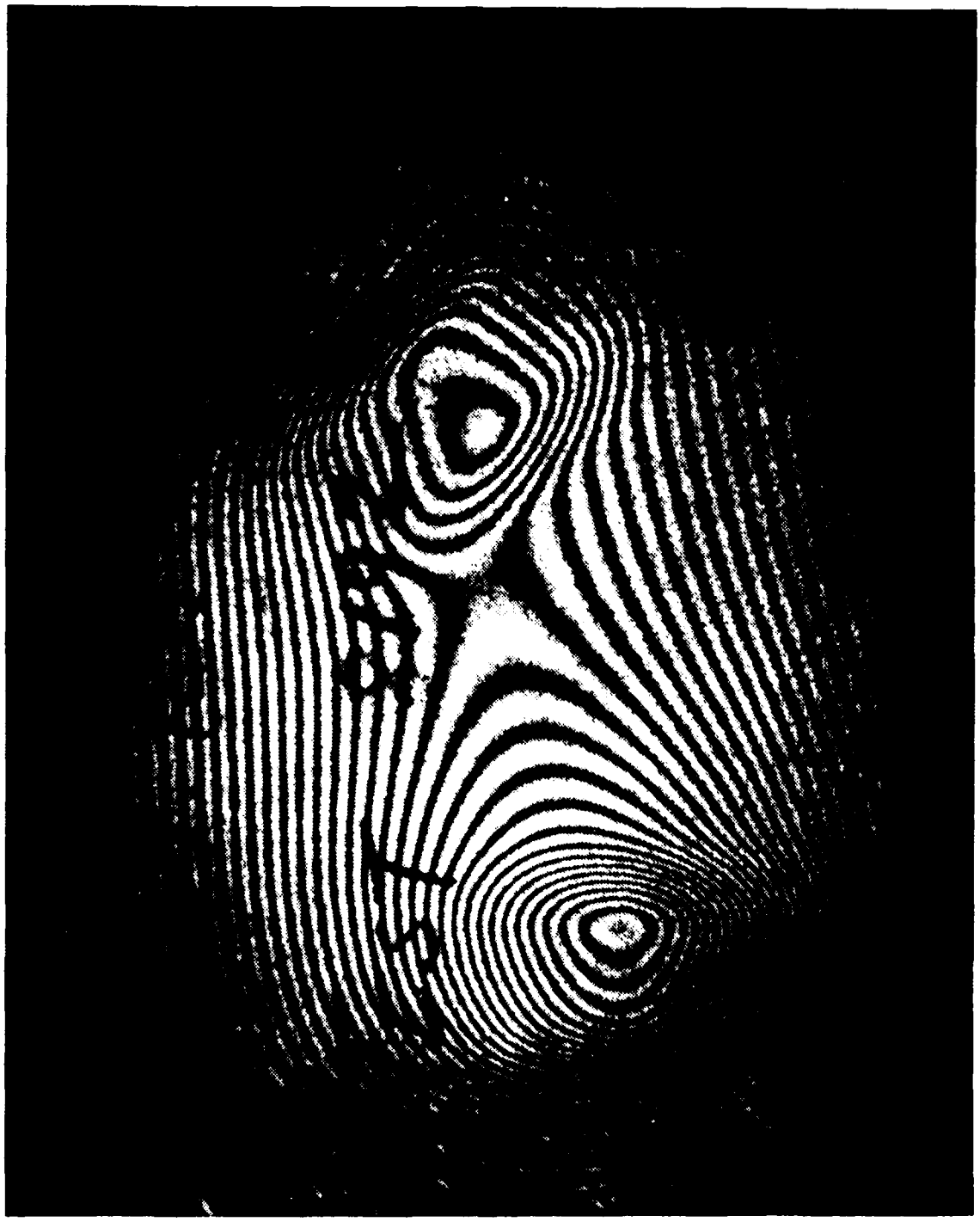

Figure 4-10. Reconstructed Image (Holographic Interferogram) from Double Exposure Hologram #1

4. The stress is removed from the plate by loosening the thumb screws and the object beam is shifted through an angle. A hologram of state #1 with the shifted beam is made as the second exposure on hologram #2. The second double exposure hologram is processed and its reconstructed image (another interferogram) is photographed. This holographic interferogram is shown in Figure 4-11. Note that the linear fringe is not seen in Figure 4-11 since the surface deformation produced by the thumb screws is much greater than one quarter wave/linear fringe period. Moireing the two interferograms shown in Figures 4-10 and 4-11 yields the desired result as shown in Figure 4-12. This experiment indicates tht the four-exposure FLI (moire) technique does indeed reduce the sensitivity of holographic interferometry and thus enables one to retain the linear fringe. This fringe would not be observable in conventional FLI (Figure 4-11).

The moire (difference) technique subtracts the common random phase between the two interferograms and emphasizes the linear fringe which was present (albeit small) in one interferogram (Figure 4-11) but not the other (Figure 4-10). The fact that the FLI fringes are not perfectly linear across Figure 4-12 means that the plate did not relax to exactly its original position. Subsequent experiments with the real time recording system and the finite element experiments substantiated this fact.

Figure 4-11. Reconstructed image (Holographic Interferogram) from double exposure hologram #2. The linear fringe is not observable.

Figure 4-12. Moire of the Two Random Noise Interferograms Indicating the Presence of the Linear Fringe

4.3.1.7 A More Controlled Experiment

After successfully completing the four exposure FLI experiment our holographic film processor from Laser Technology in Norristown, Pa. was delivered and debugged. (See Appendix B for a description of this system). This system is a real time recording system in which the holographic film is developed in place using a monobath chemistry process. Interferometry between the recorded hologram and future states of the surface can be observed in real time in the image plane. This system enabled us to perform a more controlled four exposure FLI experiment by using the following procedure:

1. A hologram of state #1 is made and processed in the real time recording system.

2. The plate was stressed by hanging weights from a lever arm attached to the back of the plate. (Note: this static loading technique was chosen because our finite element study showed that it is controllable, repeatable, and in agreement with the computer model.) This loading method removed an important random variable from our experiments. The real time holographic system enables us to vary the fringe pattern on the interferogram until high frequency noise fringes were obtained. The resulting interferogram from the real time holographic system (an interferogram between state #1 of the surface recorded on the hologram and state #2 due to the hanging wieghts) was photographed (see Figure 4-13).

3. The linear fringe was then added by swinging the object beam and another interofergram was photographed (see Figure 4-14). Again, the loading is so great that the linear fringes are swamped and hence, are not visible in Figure 4-14.

4. The resulting moire pattern obtained by moire in Figures 4-13 and 4-14 reveals the presence of the linear fringe due to the differencing technique as shown in Figure 4-15.

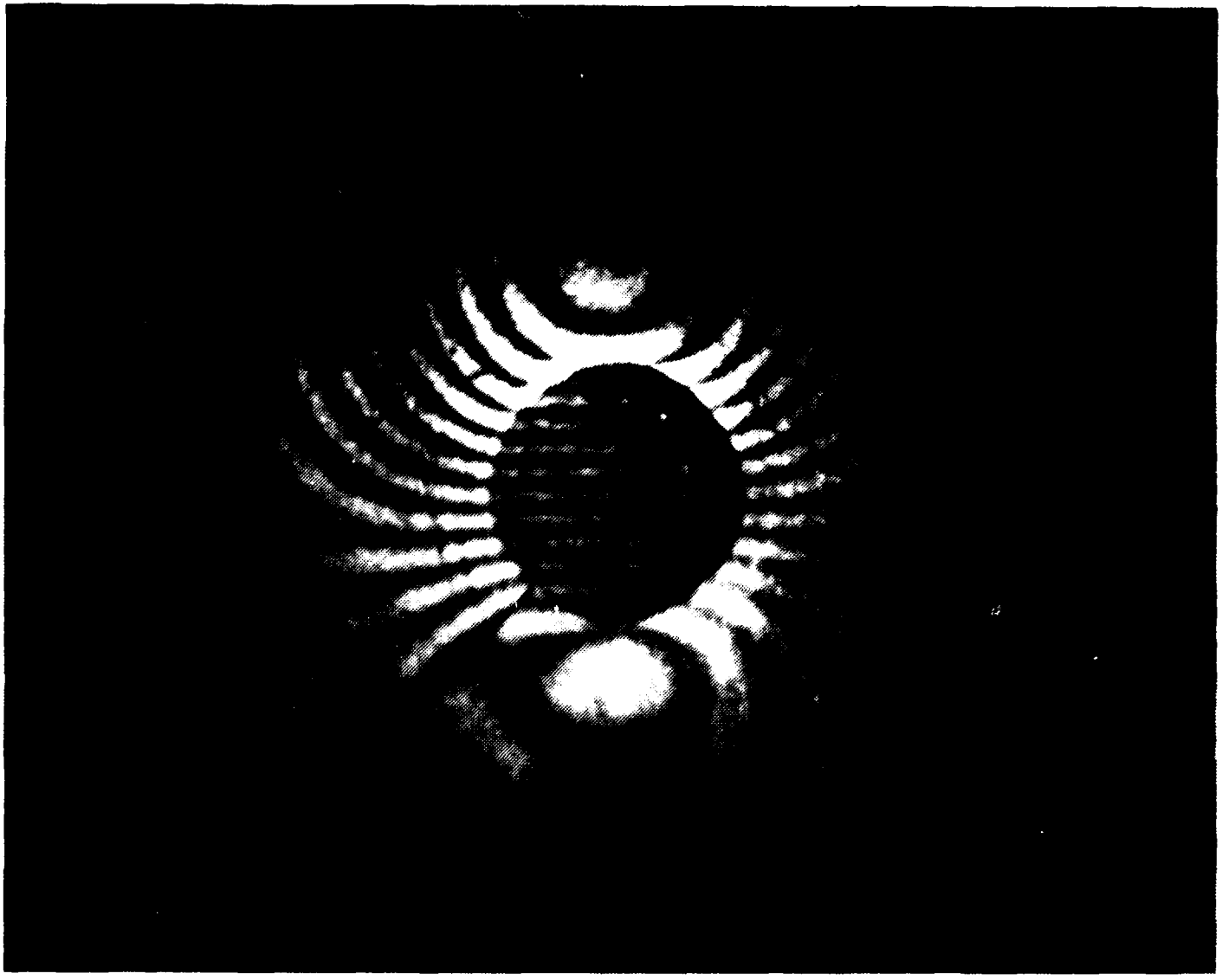

Figure 4-13. Interferogram between state #1 of test plate (relaxed), and state #2 (hanging weights) made in real time holographic system

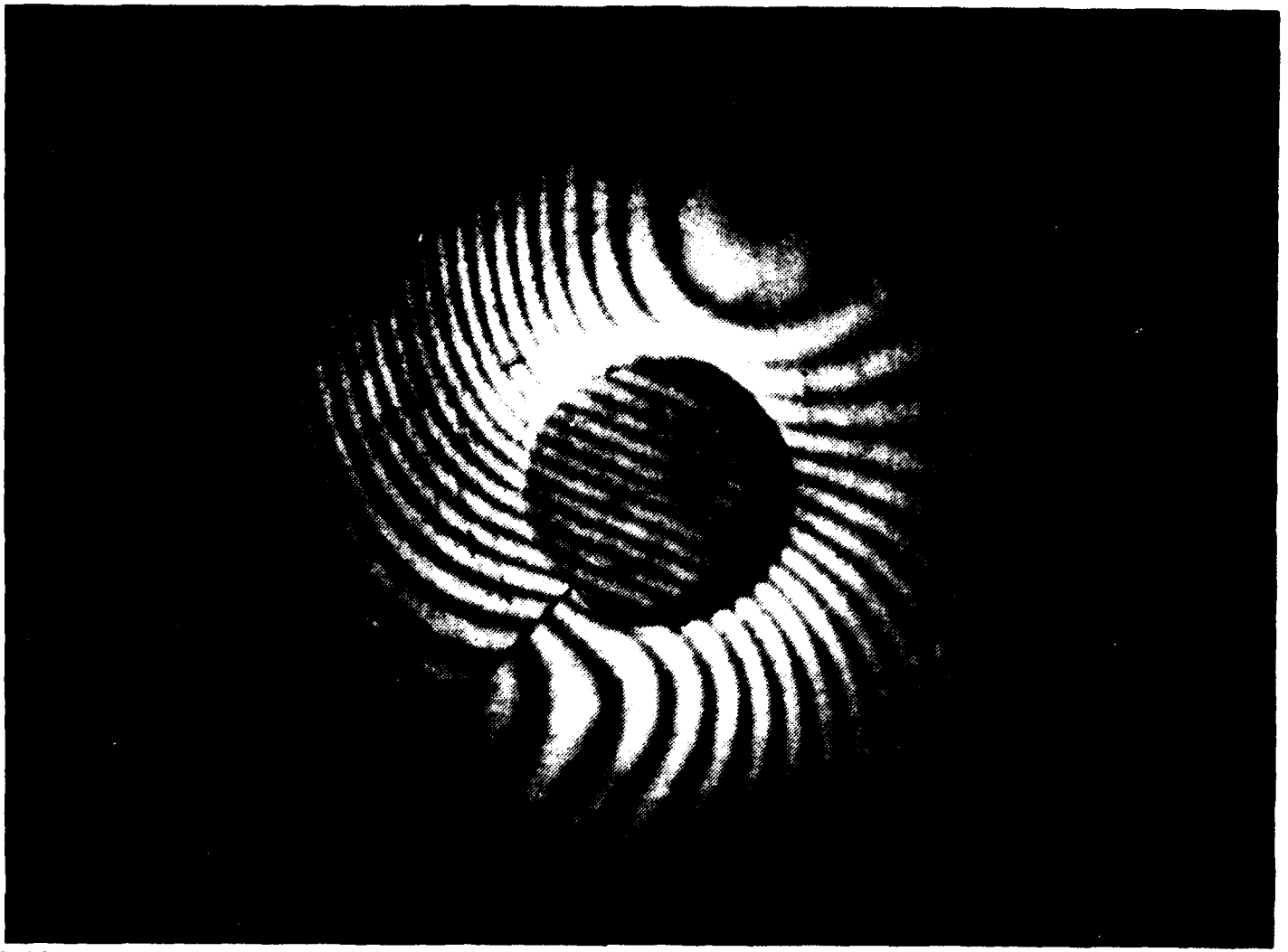

Figure 4-14. Interferogram between state #1 of the test plate (relaxed) and state #2 (hanging weights) with shifted object beam made in real time holographic system. The fringes rotate on the central plug because it is stiff and experiences a tilt from the hanging weights. Also note that the noise fringes are shifted at the position of the crack i.e., the vector addition gave a better angle of the fringes to the crack illustrating the ultimate importance of fringe direction to crack orientation

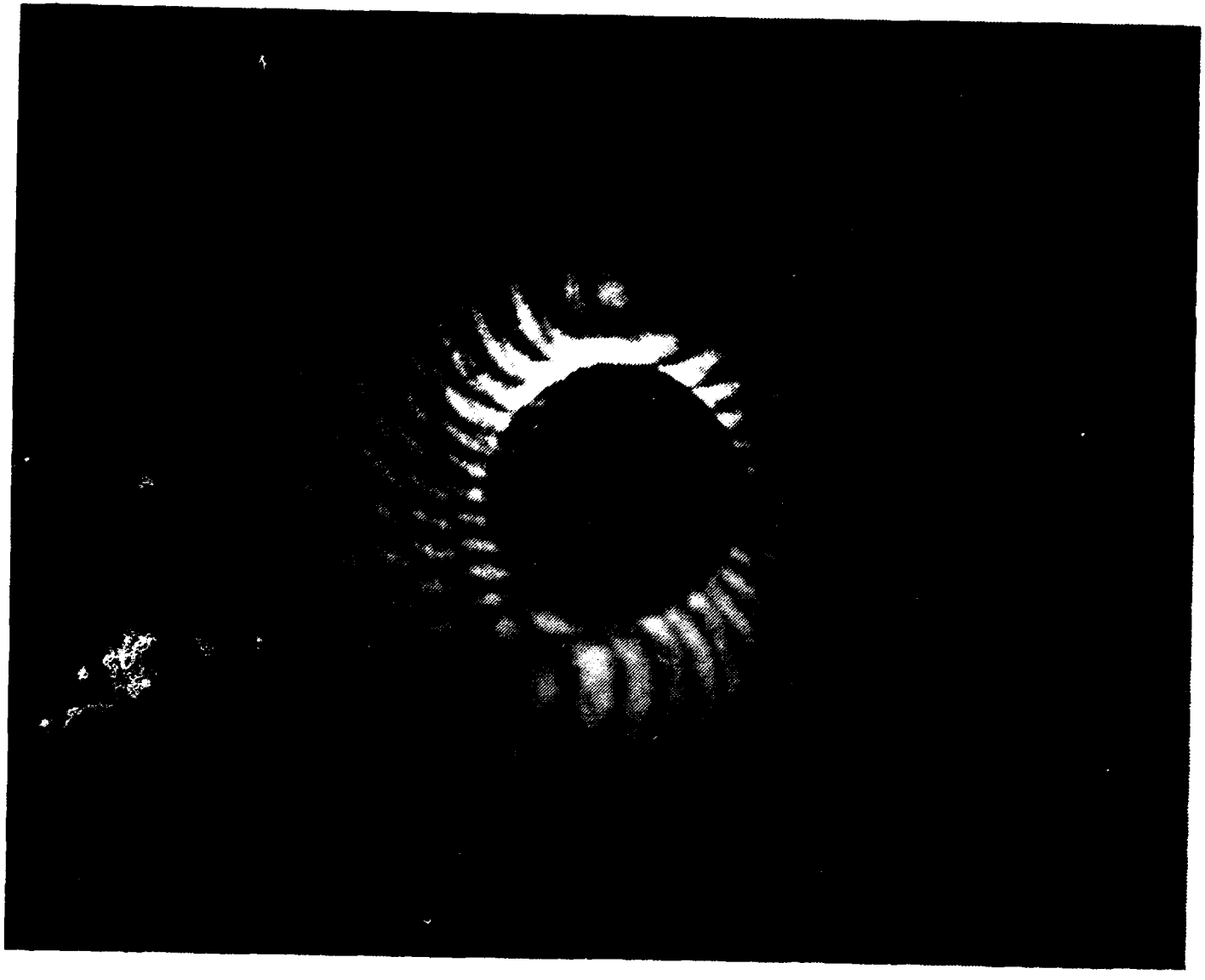

Figure 4-15. Moire of the interferograms in Figure 4-11 and 4-12 indicating the presence of the linear fringes (negative 10 degrees off the vertical).

Because the experimental controls (allowed by real time holography were better in these static loading experiments, the linear fringes in Figure 4-15 are straighter than those obtained in the earlier experiments (Figure 4-12).

Comments:

Of course in the ultimate system with two synchronous lasers and dynamic loading these concerns will not be important. In these static experiments the real time holographic system has the advantage that the desired state of the loaded system can be realized by waiting for the system to come to equilibrium after applying the force. Both interferograms are always referenced to the same recorded hologram (state #1). This removes the necessity of returning the plate to its relaxed position as we did in the initial experiment described in Section 4.3.1.6.

Real time holography shows that relaxing of the plate to its initial state, with the interferometric tolerances required, is very unpredictable due to factors such as plate fatique, etc. Thus, one has to perform many measurements and observe the state of the reconstructed image before being ensured that the plate has returned to its original state.

4.3.1.8 Four Exposure FLI and Differential Loading

The next experiment to be performed will determine if differential loading between the two states of the surface can be controlled with enough finesse to allow information about sub-surface cracks or defects to be observed as fringe shifts on the linear fringes. In the ultimate four-exposure FLI process this configuration can be realized as follows. State #1 on the surface will be realized by simultaneouly pulsing both lasers and exposing both holograms. The laser pulse effectively freezes the surface at some unknown (reference) state of the dynamic loading cycle. After a period of time, Δt, (large enough so that the state of the surface has moved many quarter wavelengths) a second exposure is made with laser #1 on holograms #1. A short time later, δt, short enough so that the surface moves less than one quarter

wave/linear fringe period out of plane, a second exposure is made with laser #2 (after shifting the object beam) on hologram #2.*

4.3.1.9 Four Exposure FLI-Static Loads

In the static differential loading experiment we will realize the differential force by adding a small additional weight to the plate, between exposures, and swing the beam to introduce the linear fringes. The interferogram resulting from this holographic process is slightly different from the one shown in Figure 4-14 since it has the differential force phase modulating the linear fringe.

This experiment is currently in progress and will be reported when it is completed.

4.3.2 Pulse Control for Circumventing Loading Contraint

4.3.2.1 The Concept

The proposed method involves taking data from a displaced plate in a short time interval (see Figure 4-16). It is hoped that the time interval, Δt will be controlled by varying the frequency and/or amplitude of the driving (forcing) function. If this is possible, then in essence, we can have large out of plane displacements but only take the data for the FLI holograms with displacements meeting the quarter-wave/fringe period restriction. This concept is being pursued in parallel with the methods just described.

*Note: This technique is greatly simplified if all four exposures are made on the same holographic plate as suggested by Varner.[8] Then the moire fringe appears as one of 16 terms in the reconstructed image and spatial filtering by the FLI process can be used to enhance the fringe contrast and reject unwanted fringe noise.

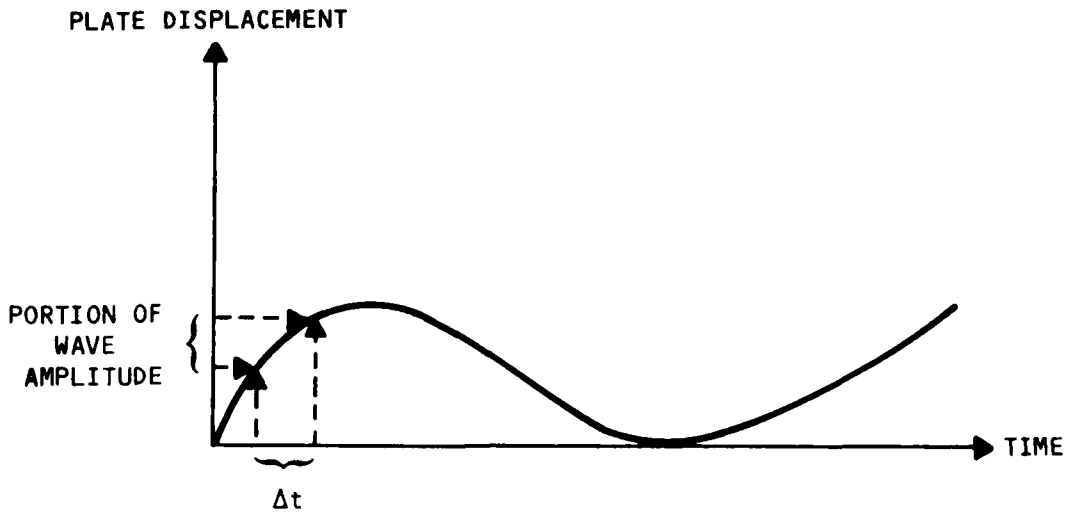

Figure 4-16. Schematic of Pulse Control Concept

4.3.2.2 **Preliminary Analysis for a Dynamically Loaded Plate**

The equation governing forced vibration of thin plates is

$$D\nabla^4 W + \rho h W = f(x,y,t) \tag{5}$$

where D is the bending stiffness $\left(\frac{Eh^3}{1-\nu^2}\right)$,
h is the thickness, and
ρ is the mass density of the plate.

If we write the forcing function, f(x,y,t) as

$$f(x,y,t) = P(x,y)e^{i\omega t} \quad ,$$

and seek solutions of the form

$$W(x,y,t) = W(x,y)e^{i\omega t} \quad , \tag{6}$$

then Eq. 5 becomes

$$D\nabla^4 W(x,y) - \rho h\omega^2 W(x,y) = P(x,y). \tag{7}$$

$$\text{Let } P(x,y) = \sum b_{nm} W_{nm}(x,y)$$

where the W_{mn}'s are mutually orthogonal and constitute the plate's natural modes of vibration, given by the eigensolutions of

$$D\nabla^4 W_{nm} - \rho h \omega^2_{nm} W_{nm} = 0,$$

where the ω_m's are the natural frequencies. It is presumed that the ω_m's are known, at least for small m and n, so that the b_{mn} are easily determined. Now $W(x,y) = \sum b_{mn} W_{mn}(x,y)$ implies

$$\sum a_{mn} \rho h (\omega^2_{mn} - \omega^2) W_{mn}(x,y) = \sum b_{mn} W_{mn}(x,y)$$

and thus

$$a_{mn} = \frac{b_{mn}}{\rho h(\omega^2_{mn} - \omega^2)} \quad . \tag{8}$$

Clearly the most attractive driving frequency would be substantially less than the lowest natural frequency. For a 4 in. x 4 in. aluminum plate, 0.1 in. thick and clamped on 3 sides, we found the lowest natural frequency to be on the order of 10^4 s^{-1}. Thus a driving frequency on the order of 5×10^3 s^{-1} would seem optimal. As may be seen from Eq. 6, the driving frequency controls the vibration frequency. With the driving frequency of 5×10^3 s^{-1}, a pulse Δt of 50 μs would cover one quarter of a cycle, while 10 ns covers only 5×10^{-5} of a cycle. Somewhere in this range we should be able to find a convenient pulse time and amplitude such that the quarterwave restriction of FLI is easily met.

By properly controlling Eq. 7, (i.e., by proper selection of P(x,y)) the lowest modes can be emphasized. This would ease calculation of the a_{mn} in Eq. 8 which would only be needed for very small m and n. Thus the amplitude can be readily estimated for the case of interest.

4.3.2.3 Initial Experiments at NADC

The purpose of the visit to NADC was to use their TRW laser Holographic system[9] and assess the system capabilities for double pulsing with short intervals between pulses.

The double-pulse system permits firing of two pulses in rapid succession, several microseconds apart. This time interval is so short that the test panel cannot experience any appreciable displacements other than the ones induced by the impact. The pulse duration is approximately 50 nanoseconds, which permits "freezing" of the motion due to the induced stress waves.

The ruby laser has the capability of producing up to four, long-coherence, optical pulses (wavelength, λ=6943Å) within one millisecond. The separation between pulses can be varied from one to 250 microseconds.

The basic components of the ruby laser are two mirrors, a ruby rod, a flashlamp, and a pockels cell Q-switch. The two mirrors form opposite ends of the optical cavity. The ruby rod provides the optical energy (light) in a coherent, monochromatic form. The flashlamp "pumps" the ruby rod, making it ready to lase. The Pockels cell is situated between the mirrors and acts as a shutter for the cavity. When the proper voltage is applied to the Pockels cell, light is allowed to pass through it forming a complete optical cavity allowing the laser to lase. When there is no voltage applied, the Pockels cell isolates one mirror from the other and the optical cavity is no longer complete.

The actual operation of the pulsed ruby laser consists of a series of steps which must be performed in the proper order. The flashlamp requires considerably more power than can be supplied on a continuous basis so it is necessary to store energy for use during the pump cycle. This is necessary to store energy for use during the pump cycle. This is accomplished by charging a large capacitor. The amount of stored energy is adjusted by controlling the voltage to which the capacitor is charged. Once the capacitor has been energized, the laser is ready to operate.

4.3.2.4 **The Timing Sequence**

The laser is fired by pumping the ruby rod with a xenon flash tube. The pumping requires approximately 1 ms. A switch on the control panel

initiates everything. The impact hammer is released as the xenon flashlamp fires. The flashlamp duration is on the order of a millisecond. After the hammer impact, the Pockels cell opens for some short interval (ns) and the laser fires. A selectable interval later the Pockels cell opens a second time and the laser fires again.

4.3.2.5 System Considerations for Experimentation

The output energy of the two beams is adjusted by tweeking pots. The capacitor voltage for the flashlamp is monitored on a scope. The scope is not fast so the pulse width is not resolvable. The pulse separation was varied from 0.1 ms to 0.2 ms. The time interval between hammer and pulse could not be measured.

At the current time the laser only fires at some ideal temperature. The laser is connected to a refrigerator that pumps water to the laser. The temperature is read out on a 1 1/2 in diameter dial indicator with about a 200 degree range - a mark every degree. The firing temperature was an arbitrary value near the 20° mark and a pencil mark was made on the panel. The laser was fired when indicator pointed to mark. Sometimes the laser fired, but not always.

An interval of 20-30 minutes was required for the laser to return to operating temperature. We did not have to align the systems, but misfires and single fires occurred often. In two days of making holograms we made eight.

We made more test shots to see if laser was firing and double pulsing than we did to make holograms.

4.3.2.6 Proposed Experiments at NADC

We can use the NADC system as currently configured to ascertain the feasibility of the pulse control technique for FLI. By controlling the time between pulses such that the surface moves less than one quarter wave per linear fringe period then the holograms should be relatively noise free and enable us to determine whether crack and flaw signatures become visible. Due

to the lack of controls on the current system, trial and error experimental methods will be used to perform these tests. These tests are planned during the fall of 1983 and will be coordinated with NADC personnel.

4.4 ANALYSES FOR FLAW DETECTION BY HOLOGRAPHIC INTERFEROGRAMS

Since the holographic interferometry technique accurately measures small surface displacements of structural components, it is capable of indicating the locations of many small cracks and flaws in stressed bodies. Flaws on or near the surface are particularly susceptible to detection by this technique, since these flaws often induce marked surface irregularities when they are stressed. The flaws, in effect, may leave a holographic signature. By comparing experimental results with theoretical analysis, this section shows the reliability of holographic displacement measurements, and the existence of a holographic signature when a flaw is present. The finite element analyses herein are based on static loading, but a separate discussion demonstrates the applicability of the results to particular cases of dynamic loading.

4.4.1 Finite Element Analysis

Finite element analyses were performed for the plate shown in Figure 4-17a, both with and without the indicated crack. This is the same basic plate as that in the previous reports on this contract.[7,10] The mesh used without the crack is shown in Figure 4-18a, and that used with the crack is shown in Figure 4-18b.

Two analyses, corresponding to the loadings in Figure 4-17b and 4-17c, were performed without the crack. The loading mechanism in Figure 4-17b proved to be an appropriate model for the hanging weight experiment, in which a weight is hung from a plug inserted in the hole, (Figure 4-17d). The weight produces an effective moment which is transferred through the plug insert to the plate. When the plate is clamped on three sides, an idealization of the moment loading by equal and opposite forces at the top and bottom of the hole leads to theoretical results in excellent agreement with the experimental interferogram, as indicated by Figure 4-19a and 4-19b. Figure 4-19a shows out of plane displacement contours from a finite-element calculation using the general purpose ANSYS program, while Figure 4-19a and all subsequent figures

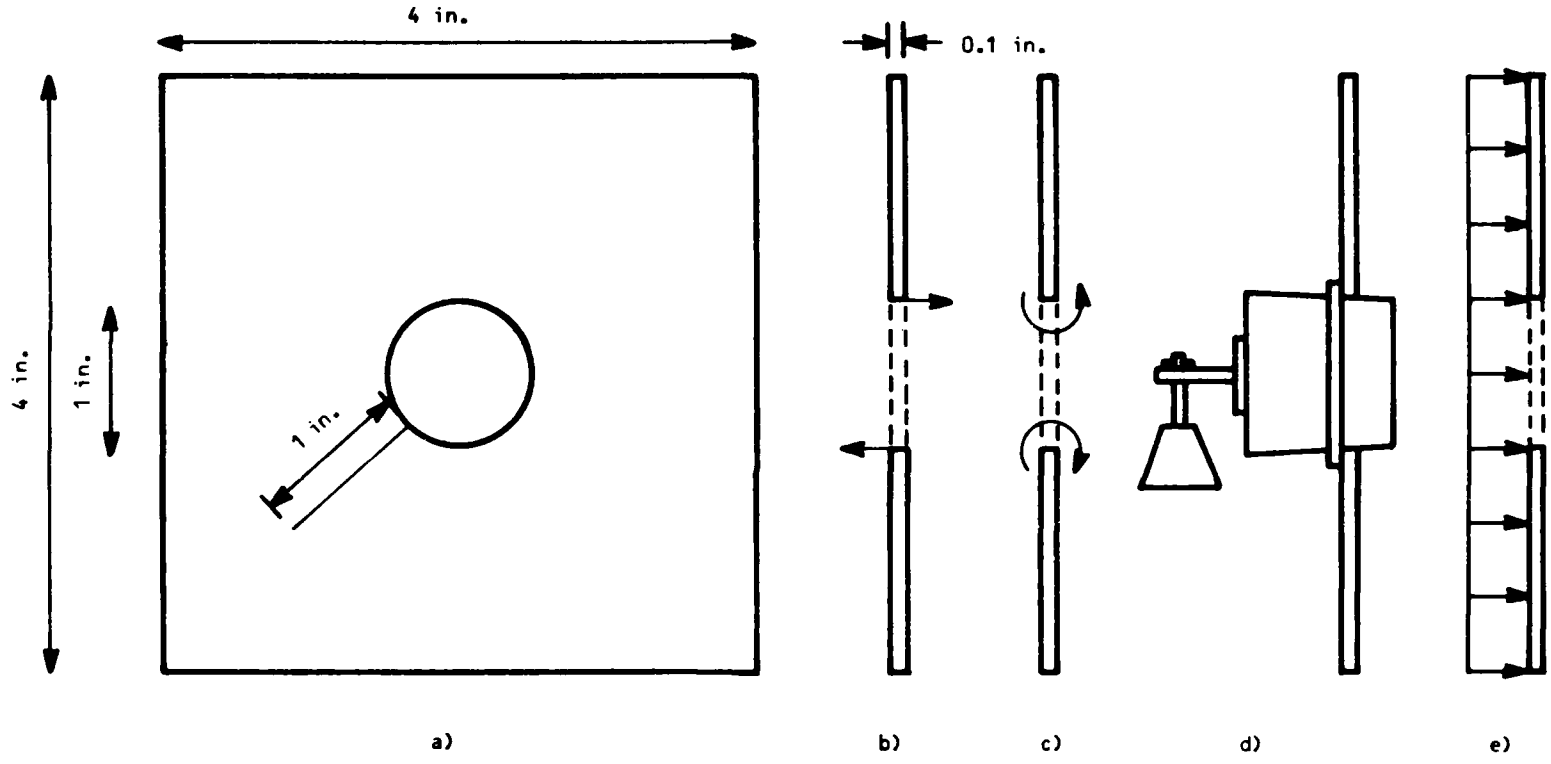

Figure 4-17a. Geometry of Test Specimen
Figure 4-17b. Force Loading Used to Model Hanging Weight Experiment
Figure 4-17c. Moment Loading Examined as Possible Model for Expanding Plug Experiment
Figure 4-17d. Schematic of Hanging Weight Experiment
Figure 4-17e. Schematic of Uniform Pressure Loading Applied to Back of Plate

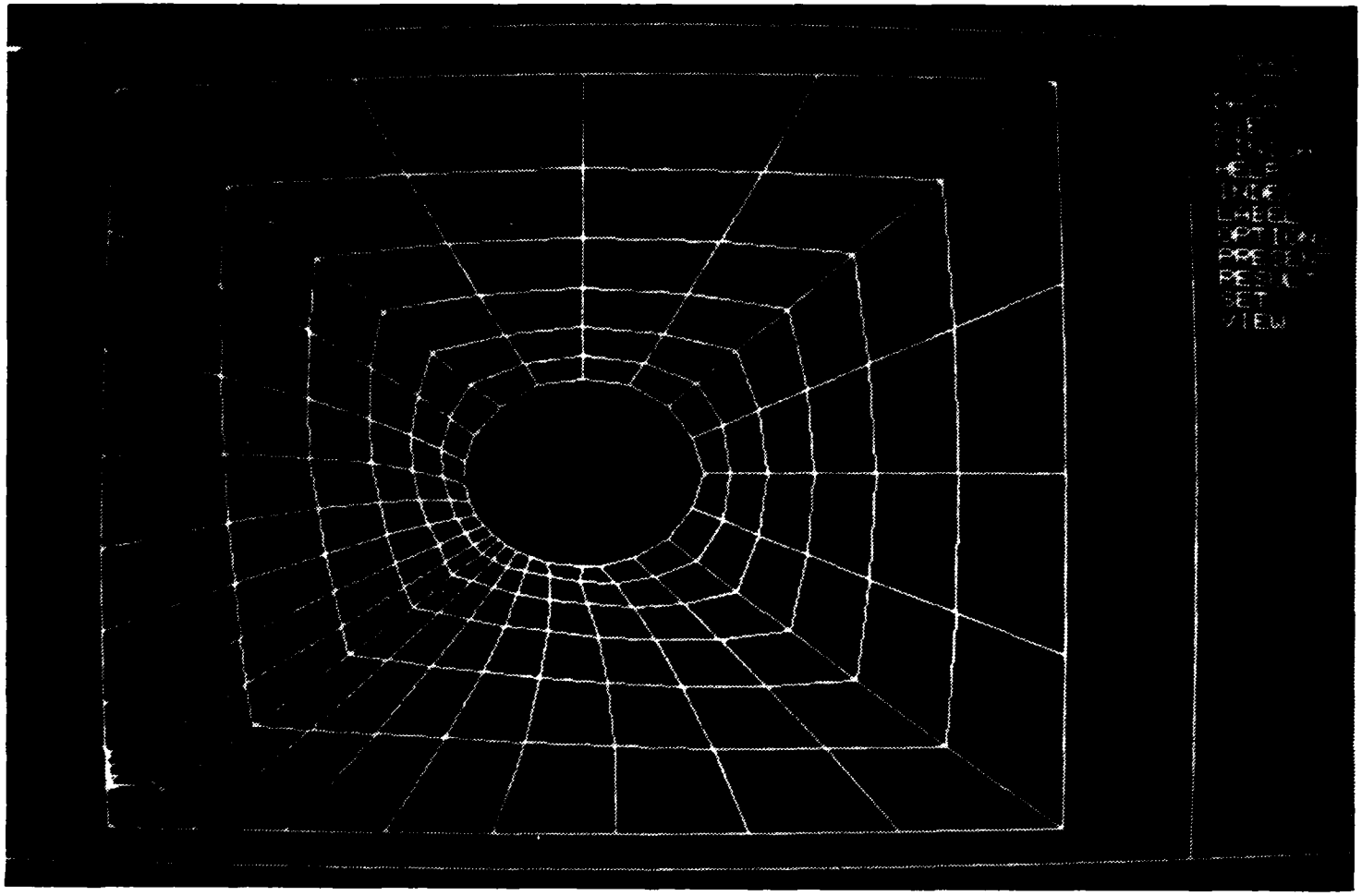

Figure 4-18a. Finite element mesh for analysis of uncracked specimens. (The computer screen has caused distortion of the figure so that the plate appears rectangular and the hole appears elliptical.)

8309-38

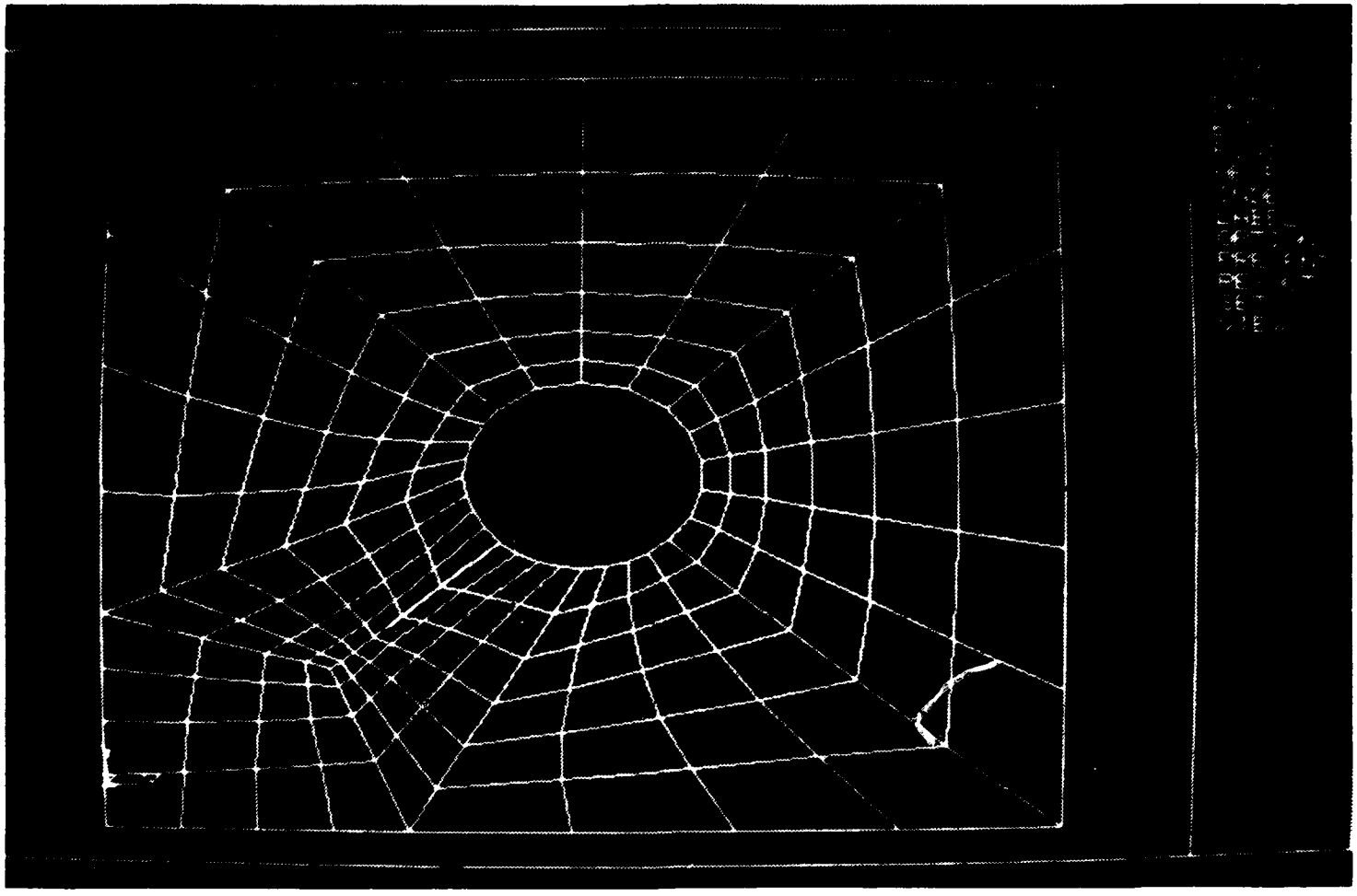

Figure 4-18b. Finite Element Mesh for Analysis of Cracked Specimens. Crack Tip is at the "Triple Point" in the Third Quadrant.

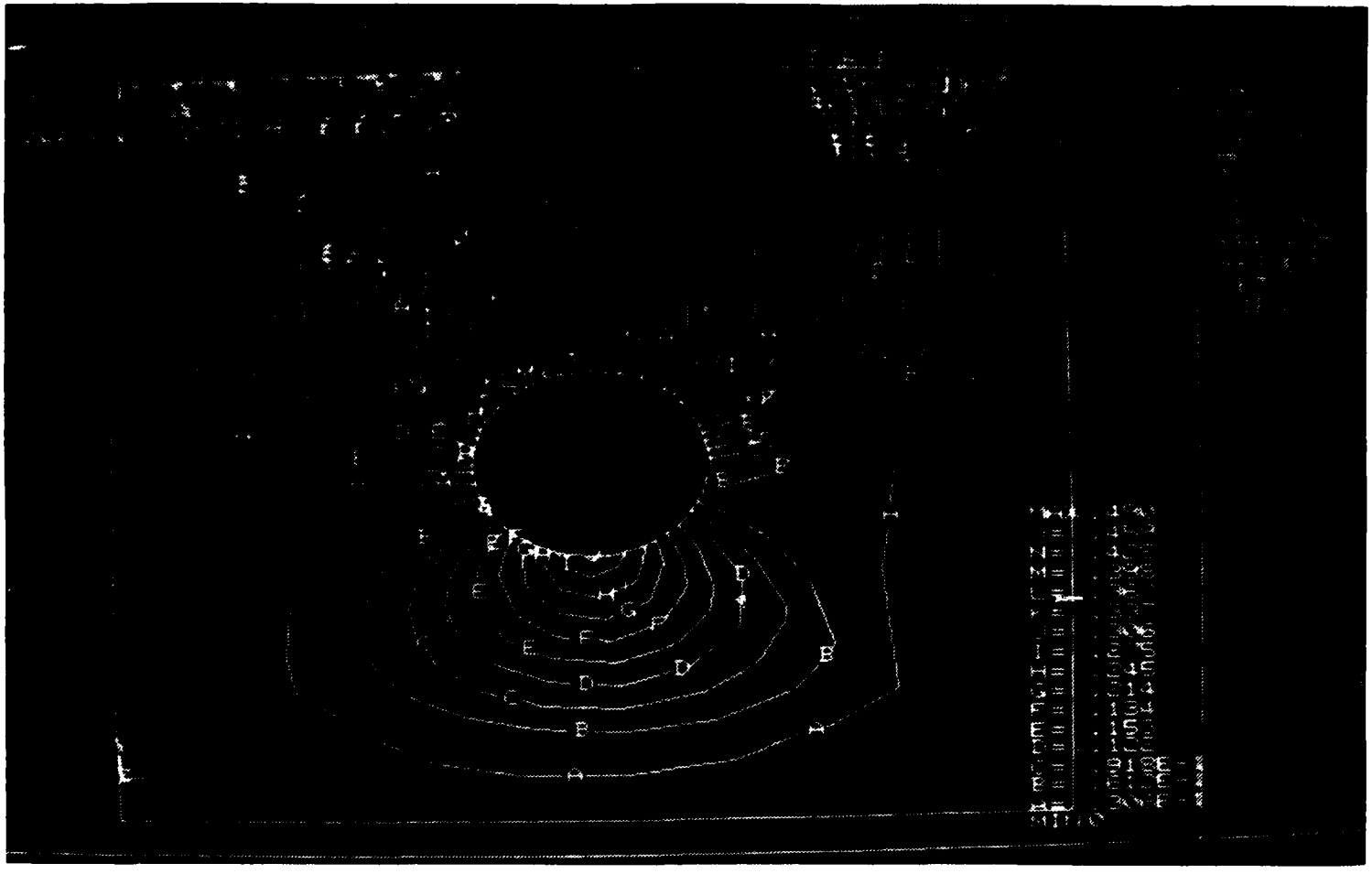

Figure 4-19a. Contours of constant out-of-plane displacement for the loading shown in Figure 4-17b. The scale at right indicates absolute displacement magnitudes. Lack of symmetry about the vertical axis is due to the same lack of symmetry in Figure 4-18a, Figure 4-18a was designed before it was known that a separate mesh would be needed for the cracked geometry (Figure 4-18b).

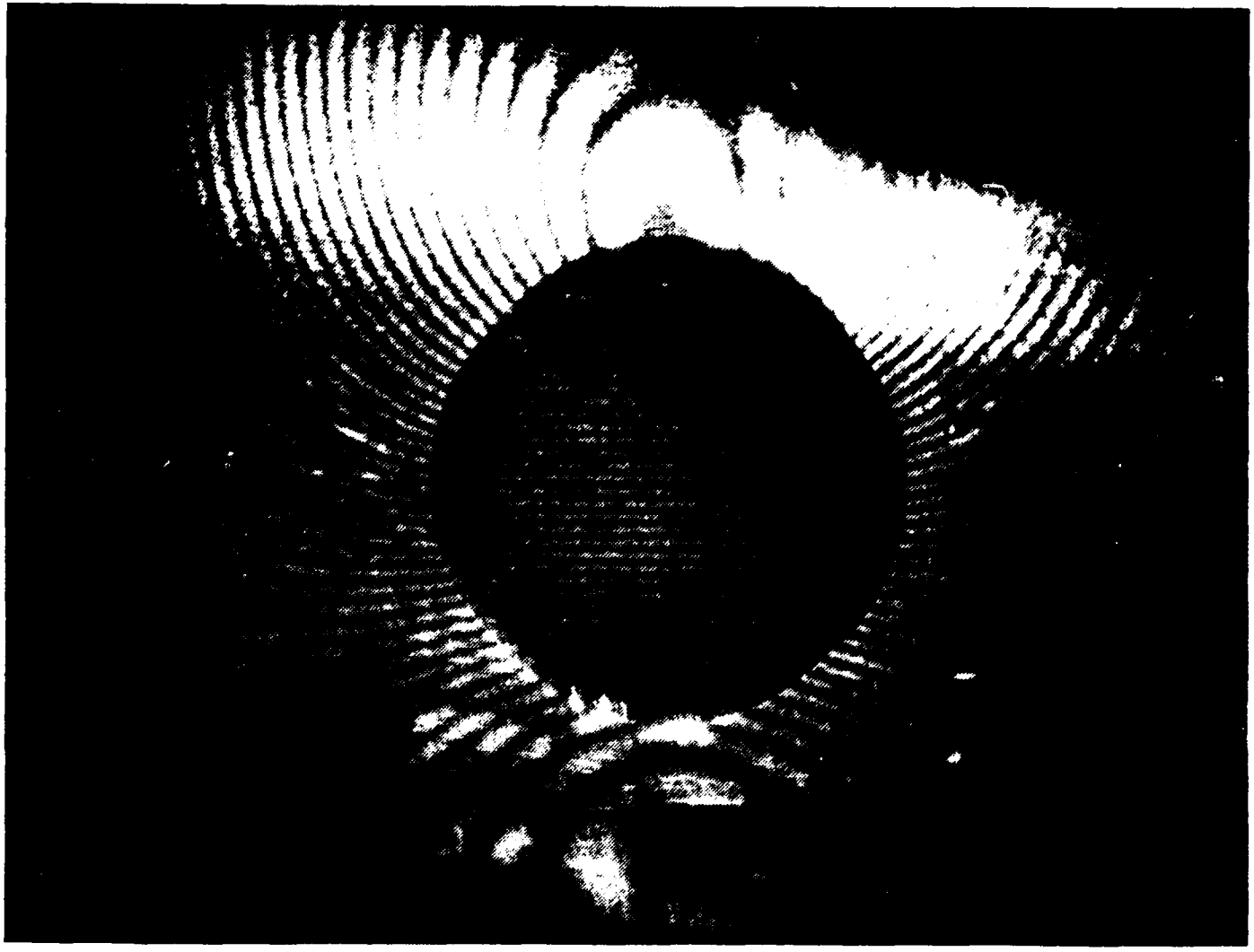

Figure 4-19b. Fringes produced in the hanging weight experiment on an unflawed specimen.

showing relative numerical results, it is important to note that absolute values of out-of-plane change actually occurs along a roughly horizontal line near the middle of the plate. Figure 4-19 thus demonstrates the holographic technique's ability to monitor surface displacements accurately.

An analysis performed for the moment loading of Figure 4-17c, which was intended to model the expanding plug experiment described in the April 1983 report,[4] did not compare favorably with either the expanding plug experiment or the hanging weight experiment (see the finite element displacement contours in Figure 4-20). Therefore, the force loading mechanism of Figure 4-17b was used in subsequent analyses in which a crack is present.

In Figure 4-21, the crack is introduced and finite element results for the same loading and boundary conditions as in Figure 4-19a are obtained. The points where the crack intersects the hole are constrained to have the same out of plane displacement to simulate the effect of the plug insert. As the closeup view in Figure 4-21b shows, the displacement contours are discontinuous at the crack, and they also exhibit a change in slope. Thus the crack has a clear holographic signature, and one would expect a similarly obvious signature in most similar applications with out of plane loading. A hologram made with a similar loading is shown in Figure 4-21c. The same general pattern is obtained as in Figure 4-21a except the holographic fringe frequency is different.

An additional example of a crack signature is provided in Figure 4-22. Here, uniform pressure is applied to the back of the plate, as depicted in Figure 4-17e. The plate is clamped on three sides as before, and again the points where the crack intersects the hole are constrained to have the same displacement, as in Figure 4-21. The displacement contours do not show a marked discontinuity across the crack, although they do exhibit a pronounced change in slope. The coupling of the points where the crack intersects the hole was next eliminated to see if the crack would cause a greater discontinuity. This lack of constraint is a reasonable assumption in light of the fact that the type of uniform pressure loading considered would arise from a loudspeaker or similar device, for which the plug insert would not necessarily be present. The results for this unconstrained case are shown in Figure 4-23, where the anticipated exacerbation of the discontinuity is clear. Since a loudspeaker is appropriate for nonstatic loading conditions, the results in Figure 4-23 also suggest the type of behavior that one might expect in a

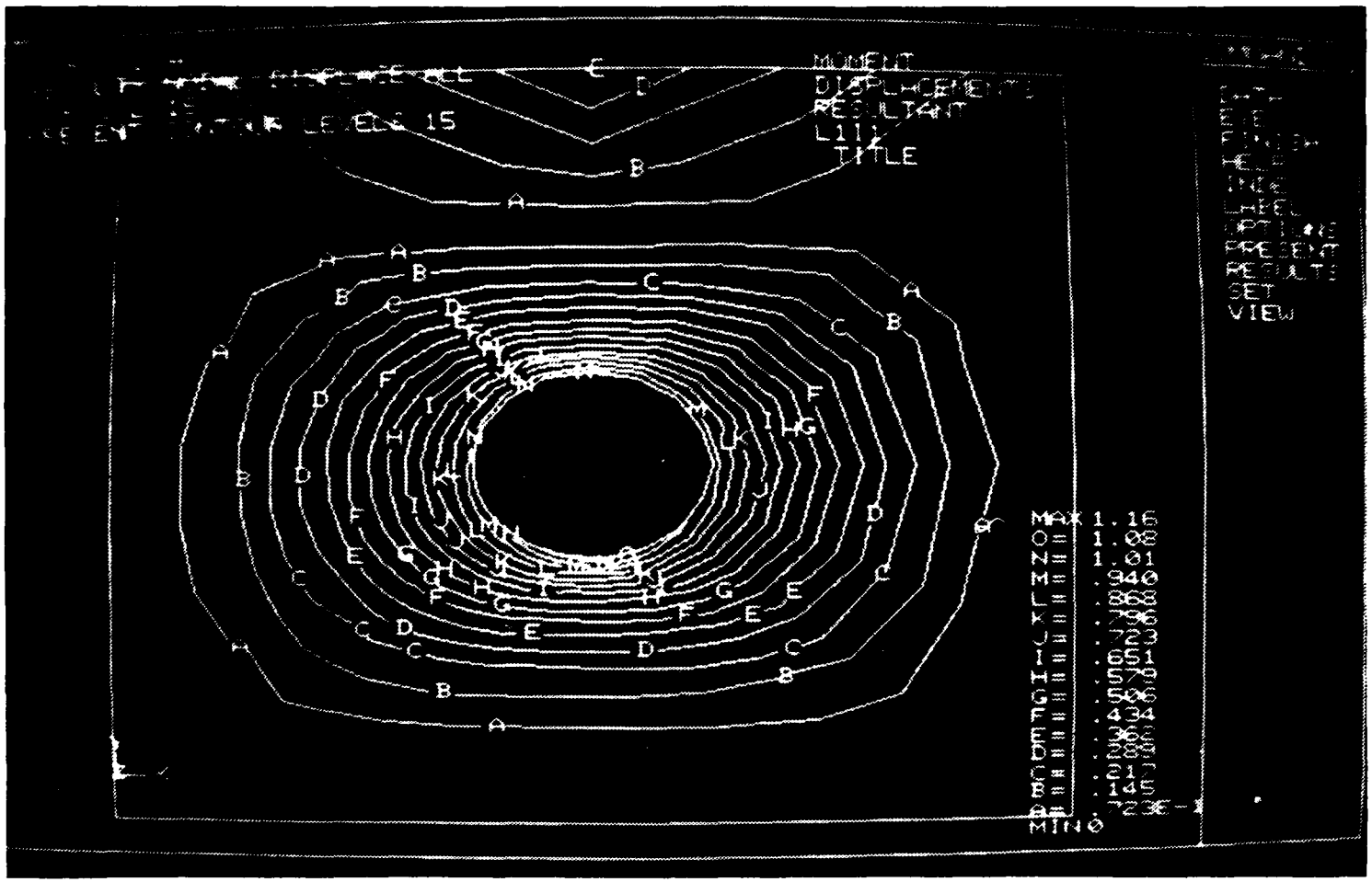

Figure 4-20a. Contours of constant out-of-plane displacement for the loading shown in Figure 4-17c

Figure 4-20b. Fringes caused by the expanding plug in an unflawed specimen

8309-38

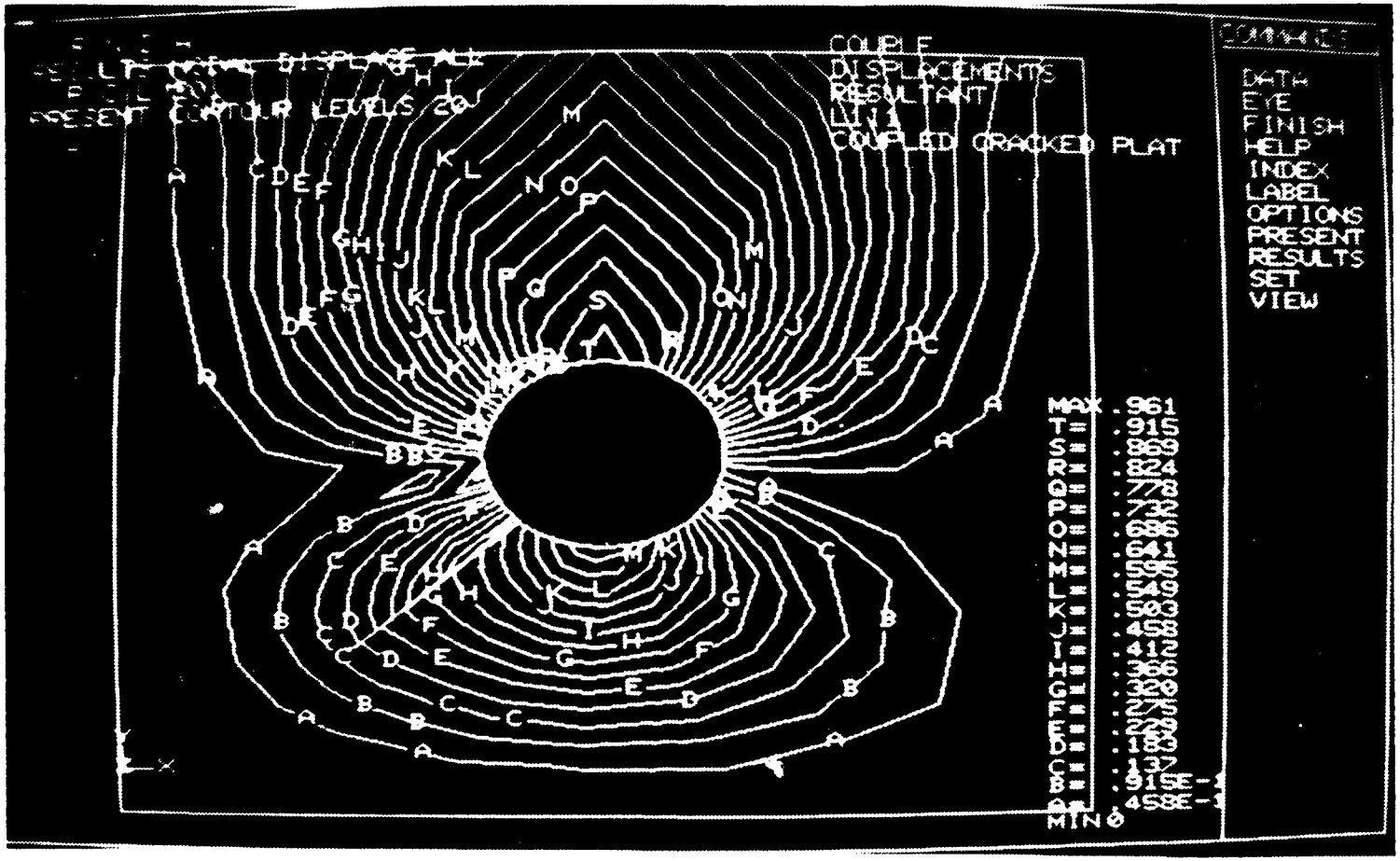

Figure 4-21a. Contours of absolute out-of-plane displacement for a cracked plate loaded as in Figure 4-17b. Displacements at the crack mouth are coupled.

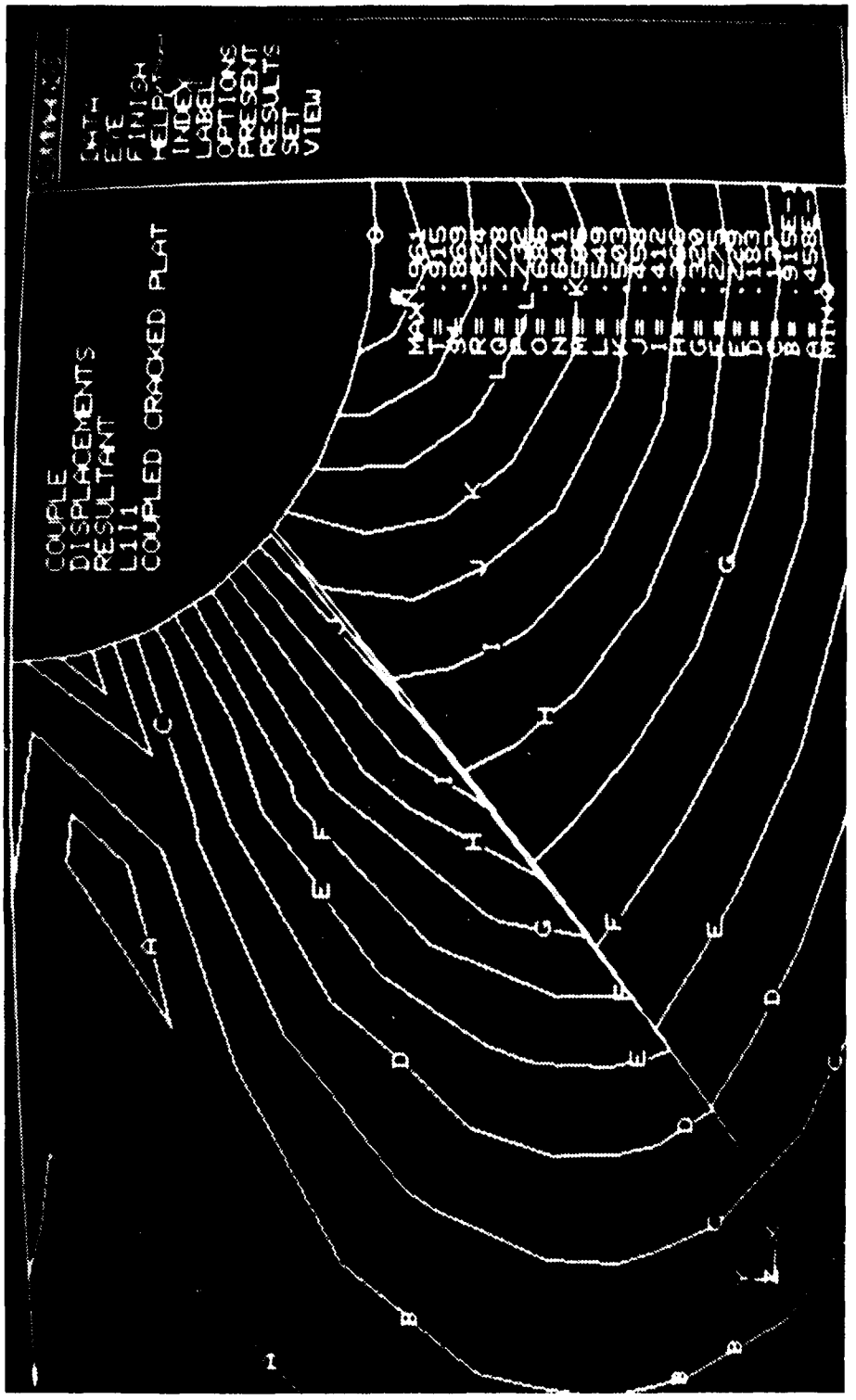

Figure 4-21b. Detail of third quadrant of Figure 4-21a.

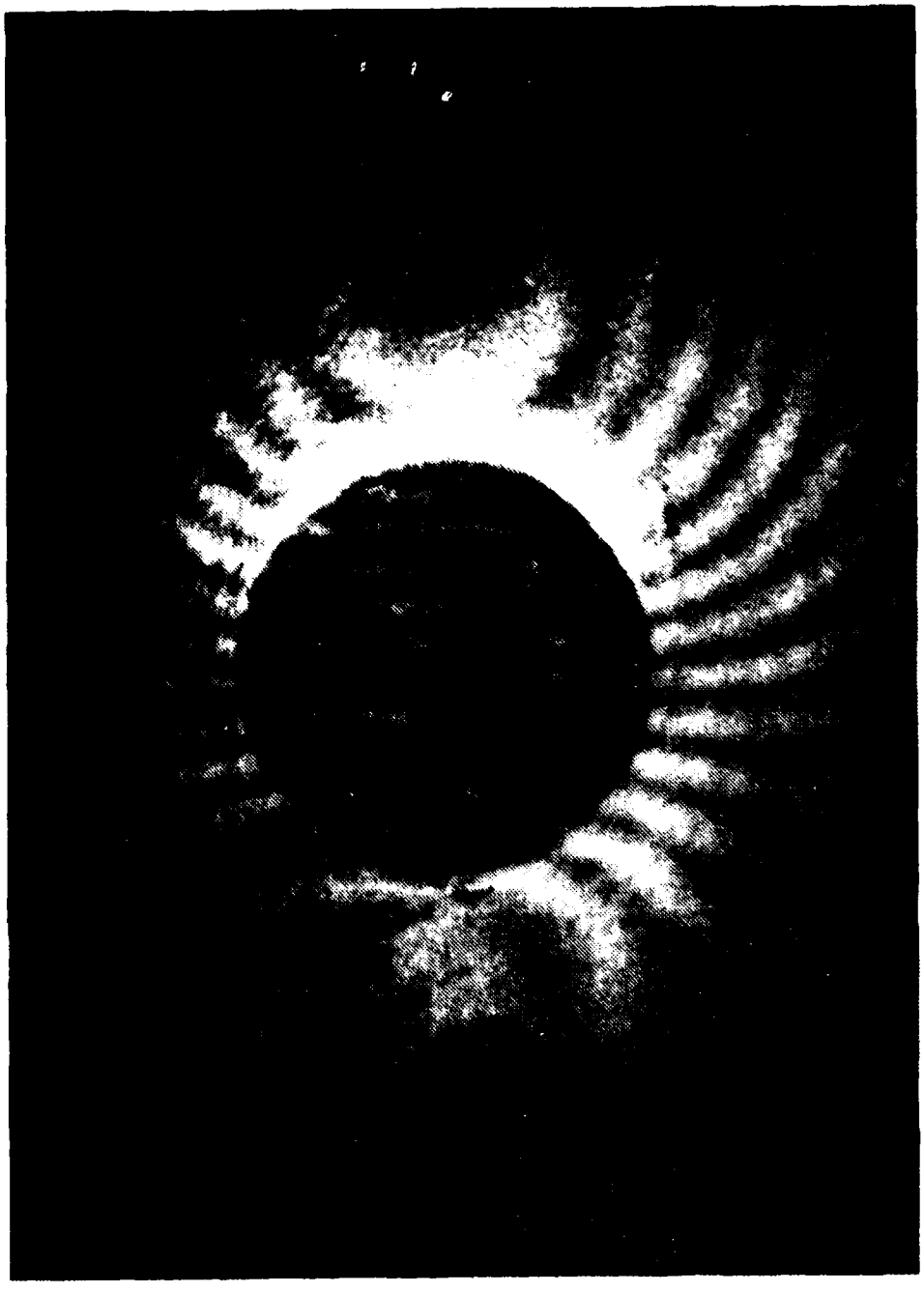

Figure 4-21c. Fringes produced in the hanging weight experiment with a flawed (through crack) specimen. Note that the amount of weight is less than that of Figure 4-19b since the number of fringes across the central circular plug is less.

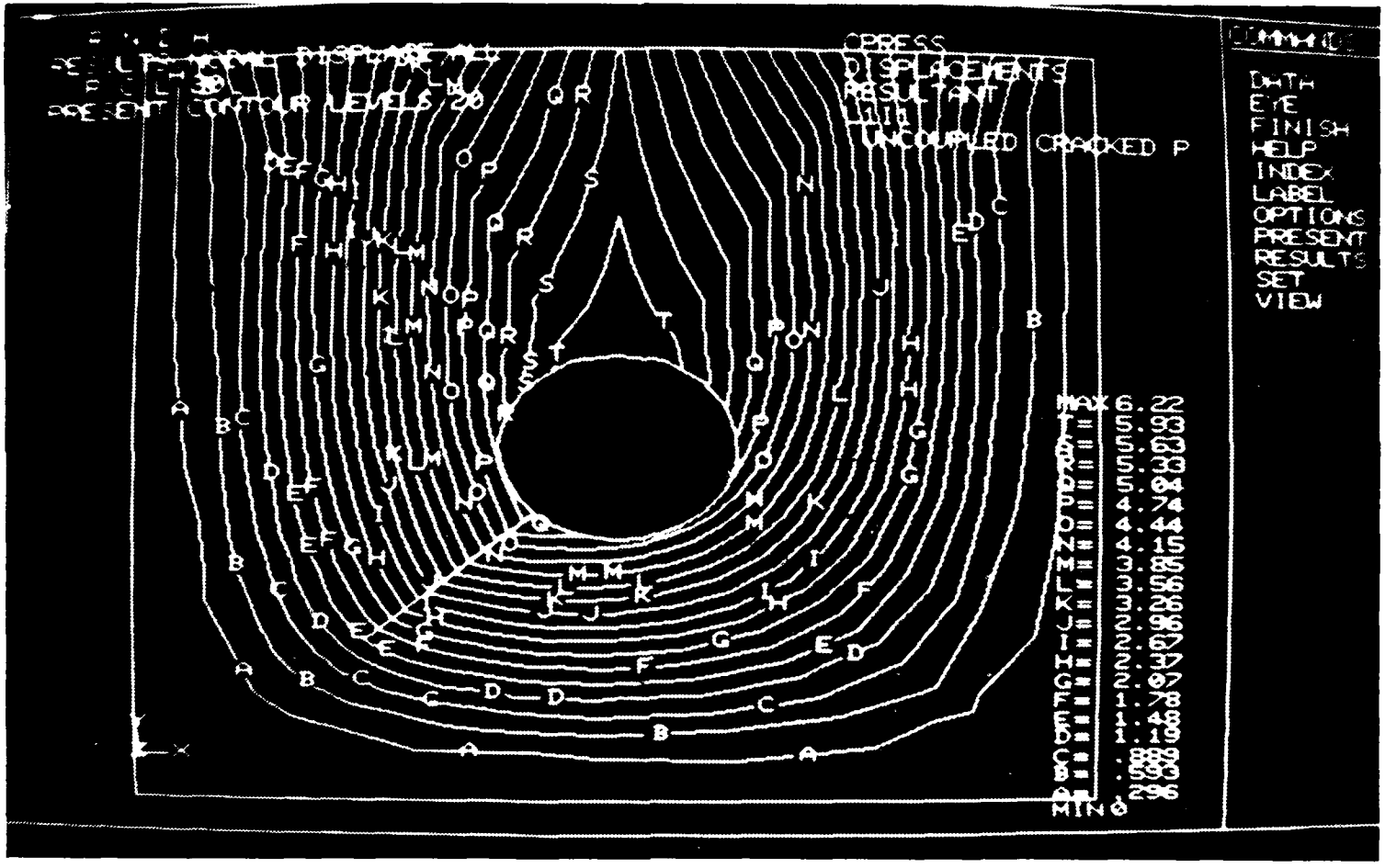

Figure 4-22a. Contours of constant out-of-plane displacement for the pressure loading in Figure 4-17c. Displacements at the crack mouth are coupled (in spite of the title in the first quadrant.

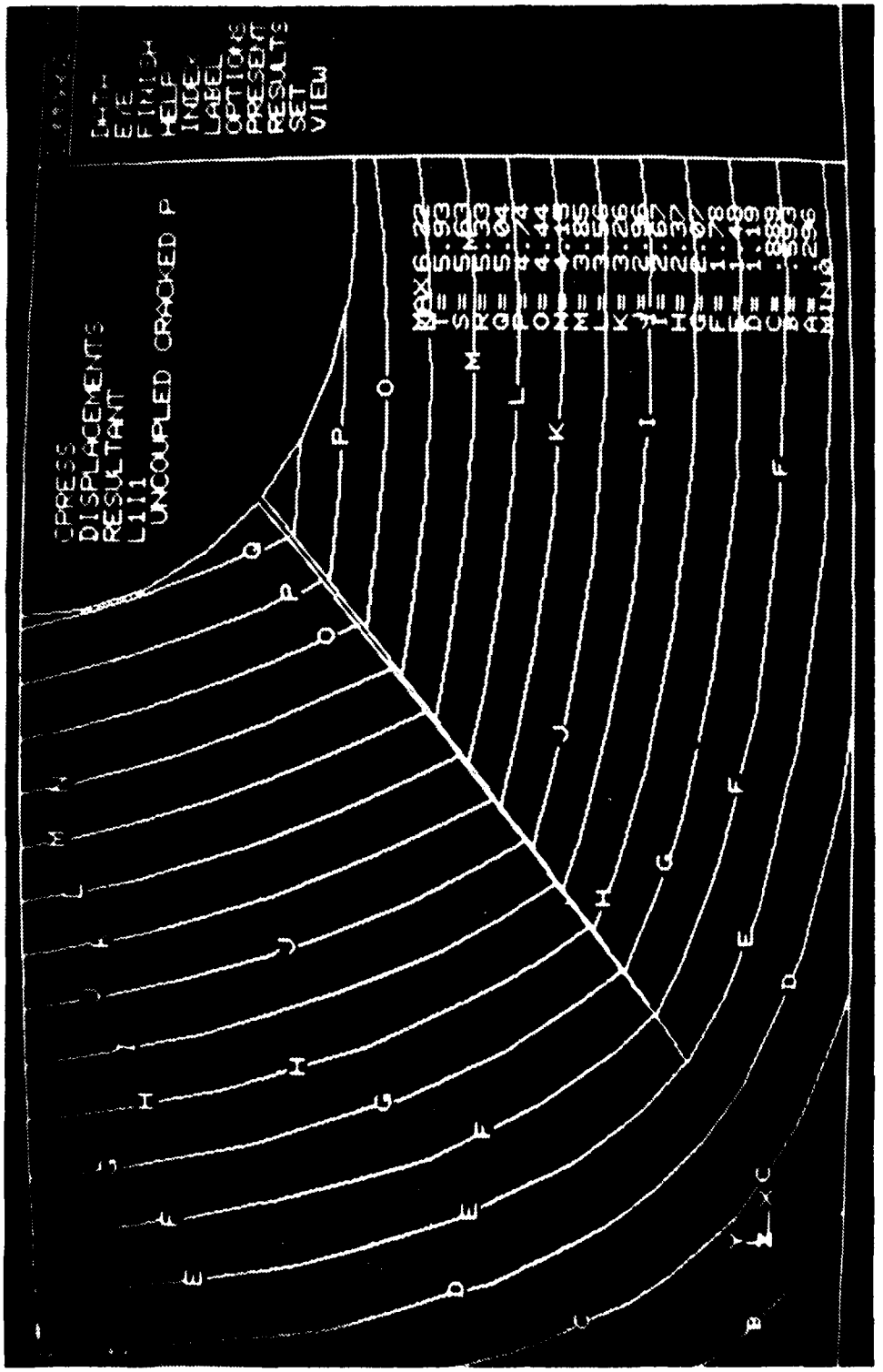

Figure 4-22b. Detail of third quadrant of Figure 4-22a

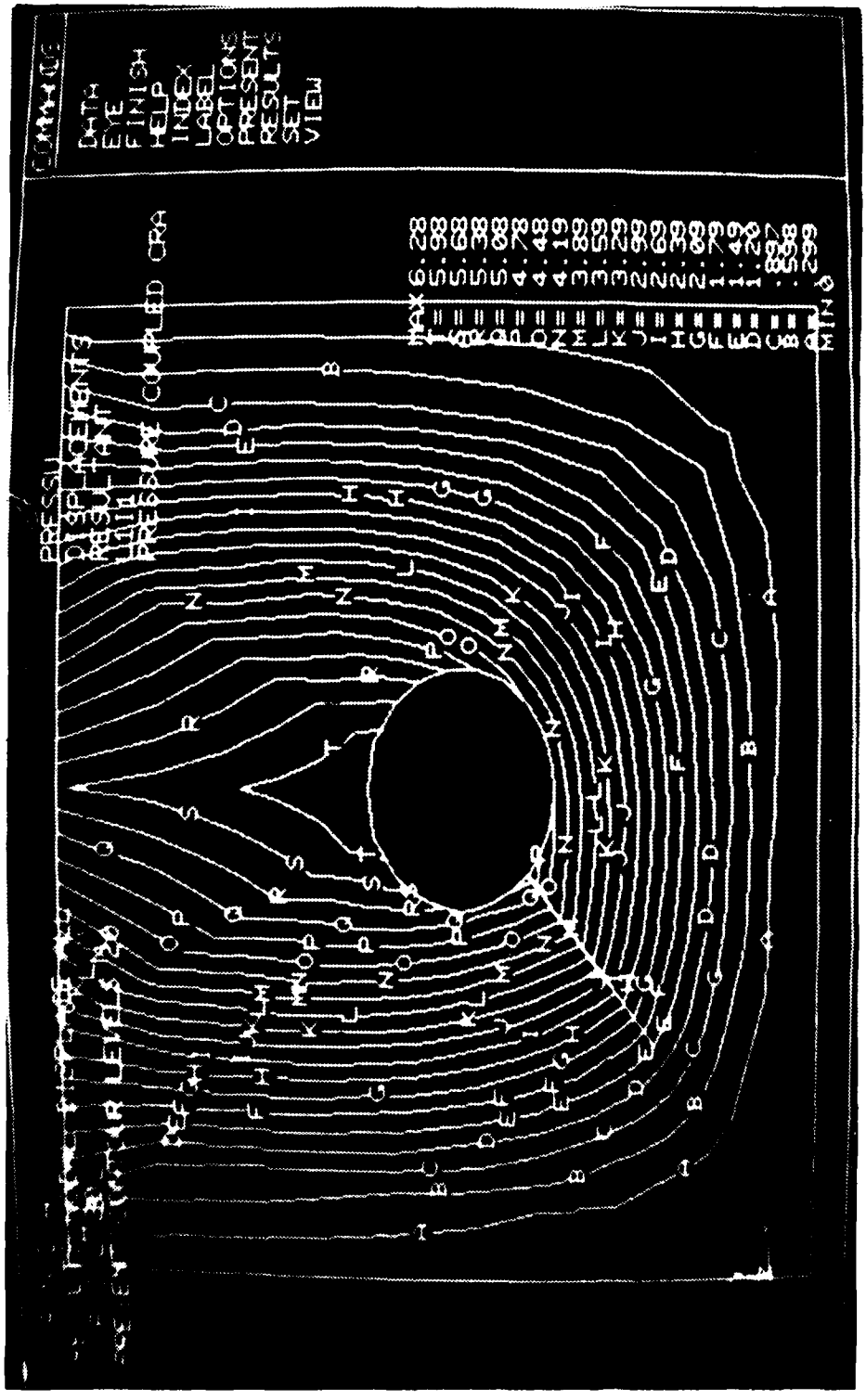

Figure 4-23a. Contours of constant out-of-plane displacement for the pressure loading in Figure 4-17c, with displacements at the crack mouth uncoupled (again despite the title).

8309-38

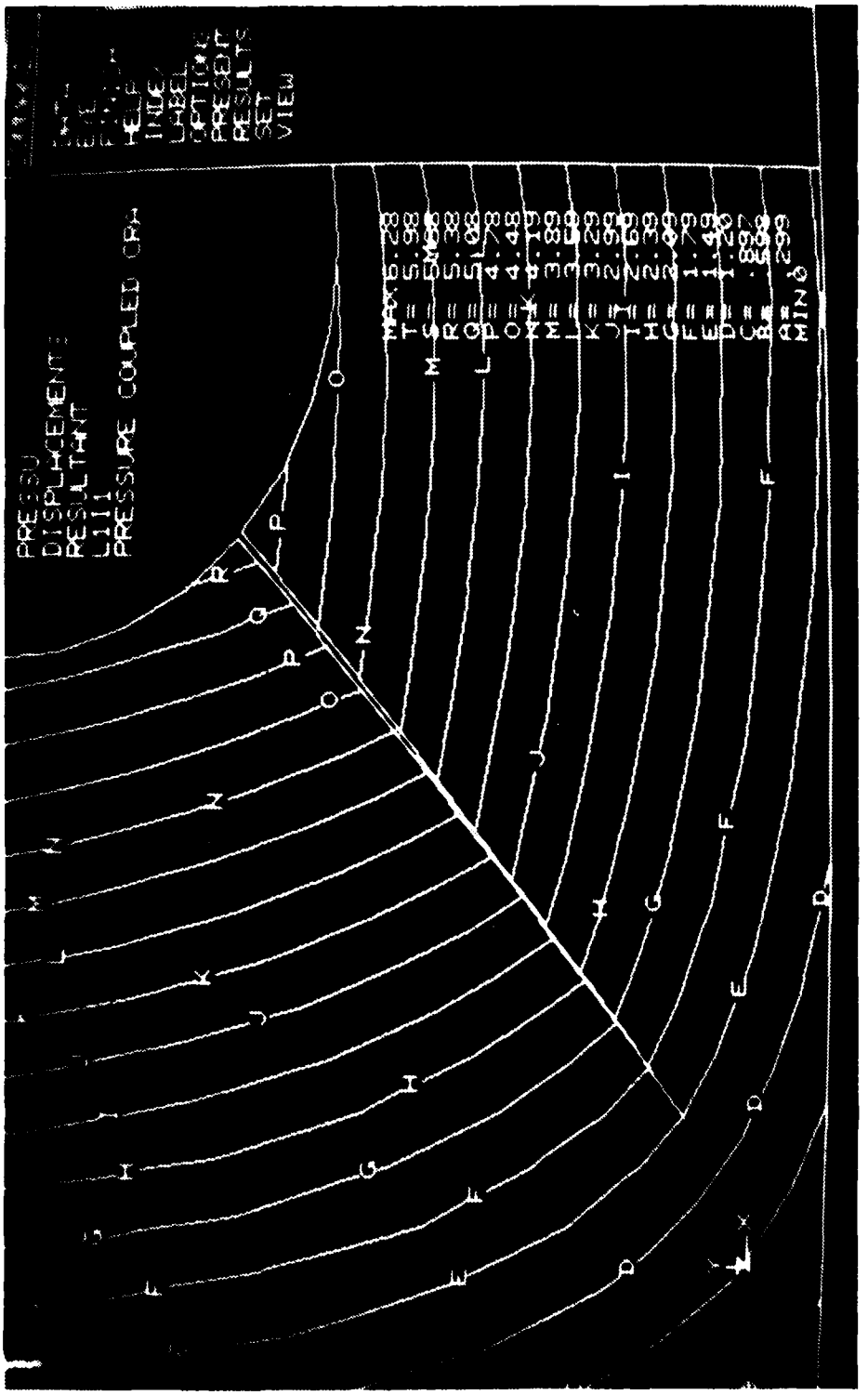

Figure 4-23b. Detail of third quadrant in Figure 4-23a

dynamic situation. The discontinuities associated with the crack are readily apparent in Figure 4-23, and one would expect similar ease of detection with an actual hologram.

4.4.2 Dynamic Considerations

In order to design an experiment which will verify the applicability of the holographic technique in a dynamic situation, an understanding of the appropriate frequency and power range for the plate of Figure 4-17a is needed. On the basis of Figure 4-23, it is understood that an easily observable crack signature will be forthcoming under the appropriate driving conditions. This section provides an approximate analysis to guide the selection of driving power and frequency.

The plate of Figure 4-17a is first idealized as flawless, i.e., as having neither a crack nor a hole. It is assumed that these flaws have minimal effect on the low frequency plate response. The boundary conditions of three clamped edges and one free edge are maintained. For purposes of discussion, we also assume a desired displacement range is specified for the driven plate, and we characterize this range by B, the maximum displacement in inches of the midpoint of the free edge. We seek to obtain driving parameters for the plate in terms of B and the other plate characteristics: Young's modulus E, Poisson's ratio, ν, density, ρ, side length, ℓ, and thickness, h. The plates bending stiffness, D, is given by

$$D = \frac{Eh^3}{12(1-\nu^2)}$$

The natural frequencies ω_i and mode shapes $W_i(x,y)$ (the W_i's are dimensionless and defined to have the value unity at the middle of the free edge) satisfy the equation

$$D\nabla^4 W_i - \rho h \omega_i^2 W_i = 0$$

The eigenvalues ω^2_i are determined by requiring the modes W_i to satisfy the plate boundary conditions. The lowest natural frequency for the present boundary conditions is given by

$$f_o = \omega_o 2\pi = \frac{1}{2\pi}\sqrt{559D/\rho h \ell^4} \quad \text{Hz.}$$

For ℓ = 4 in., ρ = 0.1 lb/in.^{3}, h = 0.1 in. ν = 0.34 and E = 10^7 psi corresponding to an aluminum plate, the lowest frequency f_o = 1.42 kHz. The next lowest frequency is almost three times as great. For dynamic plate experiments, driving frequencies on the order of 500 Hz seem appropriate for avoiding resonance.

It is typical of driven mechanical systems that there is a transient response that depends on the initial state of the system, and this response is typically damped out in a relatively short time. We assume this to be the case here so that the long time (or steady state) response derives directly from the driving mechanism. We further assume that the plate vibrations are adequately approximated by the first natural mode shape w_o.

The total energy of this mode can be calculated to be 1630 B^2 in./lb = 184 B^2 Joules. Now in the low frequency range, most of the energy of the system response is lost to damping during each cycle, and the driving force must persist if vibrations are to continue. Each driving pulse contributes potential energy to the system, which is subsequently damped without a significant amount being converted to kinetic energy. Thus the energy of the system response may be identified with the energy input each cycle, and the power required to drive the plate with displacement amplitude B is approximately 184 $B^2 f$ watts, where f is the driving frequency (Hz).

Alternatively, if the pressure providing the excitation is desired in terms of its magnitude p at the middle of the free edge, it may be estimated as follows. First, assume the pressure distribution to take on the shape of the lowest mode ω_o (this is essentially equivalent to the assumption that the lowest mode ω_o dominates the response). It may then be shown that

$$P = \rho h B(\omega^2_o - \omega^2) \approx \rho h B \omega^2_o \text{ for } \omega << \omega_o,$$

where ω is the angular frequency at which the plate is driven. These results provide the needed guidance for selection of appropriate equipment for dynamic plate experiments. For example, if the desired displacement amplitude is B, a loudspeaker device providing a frequency of 500 Hz and power input of 92 B^2 kW to the specimen would be an appropriate driving mechanism for the experiment.

SECTION 5
RESULTS TO DATE

The program goal of demonstrating a holographic NDE method which possesses a simplified data reduction technique is still possible. The original method envisioned, holographic FLI, was shown to have a severe loading constraint. Violation of this loading constraint (the common occurrence) removes the advantage obtained by spatial filtering the hologram, which was to simplify the automatic readout program. A subsequent analysis of the loading constraint led to the investigation of two methods which satisfy the constraint and appear practical. These methods are:

- Laser pulse separation control coupled with dynamic loading in linear fringe, double-pulse holography and
- Moire methods for desensitizing the response of the hologram to the load.

An analysis of the pulse control method with dynamic loading indicated it to be a feasible method. Preliminary measurements at NADC show that the method could be difficult to implement on their current system.

An analysis of the moire technique showed that the technique is feasible with two separate laser sources (4-exposure, 2-laser, 2-hologram FLI) and dynamic loading. The desensitization of the moire technique relaxes the loading constraint by allowing large surface motions between pairs of exposures while simultaneously retaining the linear fringe and spatial filtering advantage of FLI. Subsequent experimentation showed that the linear fringe is extracted from the moire technique when a large loading change between exposures was made. This experiment demonstrates that the moire method is very encouraging. The definitive experiment of obtaining shifts on the linear fringes at the location of defects is still in progress.

The finite element analyses thus far have corroborated the accuracy of the holographic interferometry technique in monitoring surface displacements. It has also been seen that cracks and flaws can be expected to leave holographic signatures when these flaws are appropriately stressed. The dynamic analyses at this point serve as a guide for subsequent experiments. Such experiments will be performed in concert with steady-state dynamic finite element analyses, so that direct correlations of experiments with analyses can be made. As in the static cases described earlier, these correlations should serve to demonstrate the effectiveness of holography in measuring surface displacements, and in pinpointing the locations of cracks.

SECTION 6
FUTURE PLANS

The work that remains to be done during Phase II includes demonstrating the four exposure FLI technique with differential loading for specimens having through cracks and sub-surface cracks. The model for these situations will be utilized to predict the size and depth of cracks which can be detected and located by the moire technique and to determine its limitations. More experimentation will be conducted at NADC to determine the practicality of implementing the pulse control techniques on their system and the dynamic loading analysis will continue.

SECTION 7
REFERENCES

1. R. S. Longhurst, Geometrical & Physical Optics, John Wiley & Sons, N.Y. (1967) p. 278.

2. D. M. Meadows et al, "Generation of Surface Contours by Moire Patterns" Appl Opt 9(4)942 April (1970).

3. J. R. Varner, "Desensitized Hologram Interferometry", Appl Opt 9(9)2098 Sept (1970).

4. Optical Engineering 21(4) July-Aug (1982). Many incoherent moire measurement methods are described in this issue.

5. J. R. Varner, "Holographic Contouring: Alternatives and Applications", SPIE Seminar Proceedings, Vol. 25 (1971) p. 239.

6. N. Abramson, The Making and Evaluation of Holograms, Academic Press, N.Y. (1981) p. 222.

7. G. Reynolds et al, Annual Report on Contract F49620-82-C-0001, April 1983.

8. J. R. Varner, "The Use of Contour Maps for Measuring Surface Displacement" in "Holographic Non-Destructive Testing", ed. by R. K. Erf, Academic Press, N.Y., (1974) p. 270.

9. TRW Systems Group, "Feasibility Demonstration of Applying Advanced Holographic Systems Technology to Identify Structural Integrity of Naval Aircraft," Interim Report Contract No. N62269-72-C-0400, 23 March 1973.

10. G. Reynolds et al, Interim Report on Contract F49620-82-C-0001, October 1982.

APPENDIX A

THEORY OF FOUR-EXPOSURE, TWO-LASER, TWO-HOLOGRAM FLI PROCESS

In Section 4.2 we experimentally show that the original FLI approach is limited to out-of-plane displacements on the order of one quarter wave/ fringe period because the interferometric term of interest in holographic FLI is

$$\left| e^{i\omega_0 x} + e^{i\Delta\phi_n} \right|^2 \simeq 1 + \cos(\omega_0 x + \Delta\phi n)$$

The noise term, $\Delta\phi_n$, cannot be allowed to swamp the linear fringe term, $\omega_0 x$, since they add vectorially.

It is difficult to control the loading to this degree of finesse. However, one method, (pulse control) for possibly accomplishing the loading is discussed in Section 4.3.2 of this report. Another method is the moire technique described in more detail in this appendix.

In the holographic moire describe by Abramson[6] (see Figures 4-5 and 4-6 of this report), the moire fringe can be mathematically described by subtracting the phases of the two interferograms. i.e.

$$\omega_0 x - (\omega_0 x + \Delta_{loading}) = -\Delta_{loading}. \qquad (A\text{-}1)$$

Since four-exposure, two-hologram FLI is the opposite of the Abramson case, (i.e. noise carrier) the resulting phase is

$$\Delta_{loading} - (\omega_0 x + \Delta_{loading}) = -\omega_0 x \cong \text{linear fringe} \qquad (A\text{-}2)$$

In four-exposure FLI with a Phase, δ, due to differential loading the two double exposure holograms can be represented as

$$H_1 = \left|e^{i\phi_1} + R\right|^2 + \left|e^{i\phi_2} + R\right|^2, \qquad \text{(A-3)}$$

exposure #1 + exposure #2

and

$$H_2 = \left|e^{i\omega_0 x}\, e^{i\phi_2+\delta} + R\right|^2 + \left|e^{i\phi_1} + R\right|^2, \qquad \text{(A-4)}$$

exposure #3 and exposure #4

where ϕ_1 and ϕ_2 represent the out-of-plane displacements due to the two different forces, R is the holographic reference wave and δ is the phase resulting from the differential loading.

When these two holograms are reconstructed and moired, the moire fringe (difference frequency) is

$$\cos\,(\omega_0 x + \delta) \qquad \text{(A-5)}$$

i.e. phase shifts from the differential loading riding on the linear fringe. Since these phase shifts should be larger at the defect locations, the four-exposure FLI holograms should be more amenable to automatic readout than conventional double exposure holography.

APPENDIX B
LASER TECHNOLOGY SYSTEM

HOLOMATIC 6000

INSTANT HOLOGRAM RECORDING SYSTEM

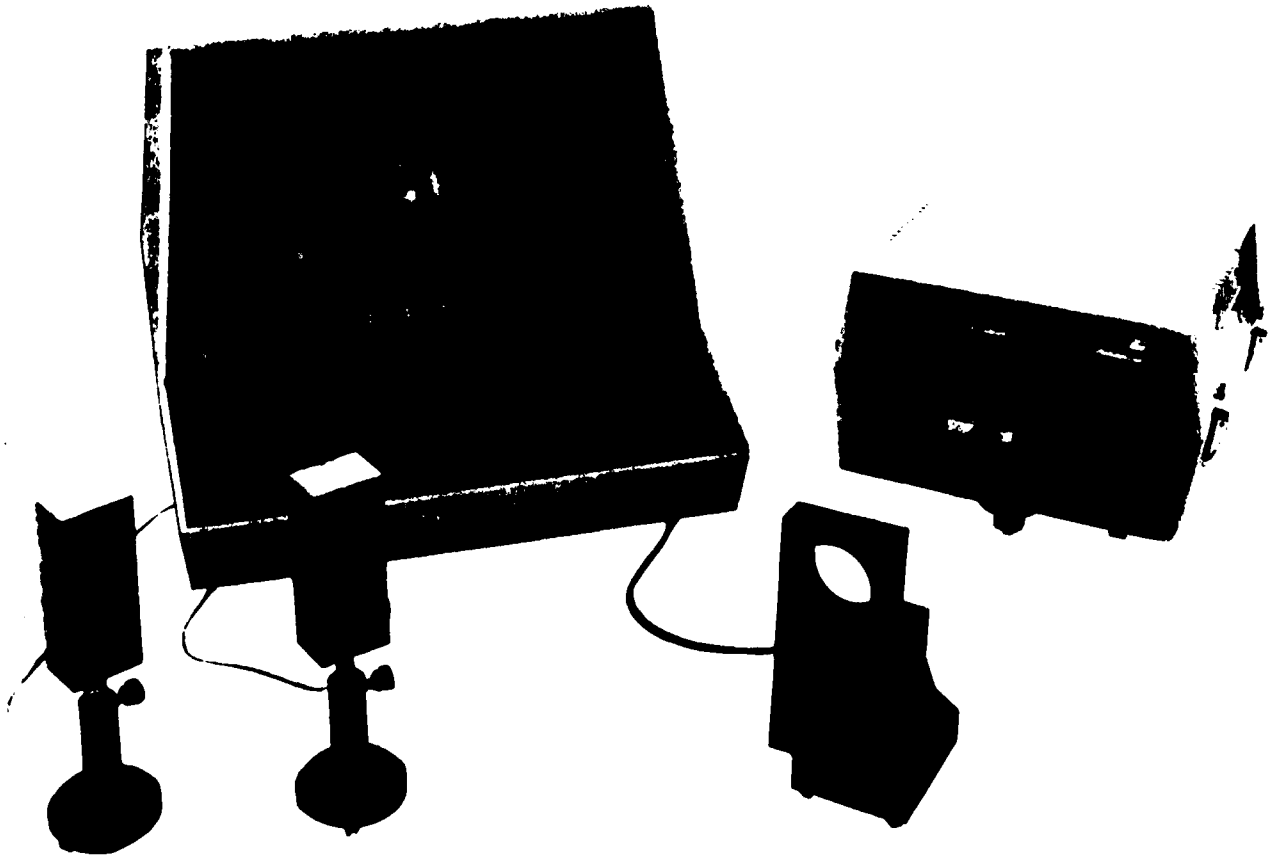

- Produce holograms in 10 seconds, up to 6 per minute.
- *Permanent* Holograms made with standard Holographic Film over a magnitude more sensitive than thermoplastic recording equipment.
- View each hologram seconds after the exposure, using the video monitor provided.
- Microprocessor control HOLOMATIC 6000 makes REAL TIME, TIME AVERAGE or DOUBLE EXPOSURE holograms.
- Eliminate all dark room processing of holograms.

LTI™ **LASER TECHNOLOGY, INC.**

HOLOMATIC 6000 INSTANT HOLOGRAM RECORDING SYSTEM

Description

Combining the latest microprocessor technology and a revolutionary monobath processing fluid, the HOLOMATIC 6000 is the fastest and most sensitive holographic recording and production control instrument available. Programmed to produce REAL TIME, DOUBLE EXPOSURE or TIME AVERAGE holograms at the touch of a button, the HOLOMATIC 6000 opens new dimensions in holography. For modal analysis, scan the test part through a range of vibrational frequencies with any shaker and oscillator. The REAL TIME hologram will show the modal patterns moving and changing as the frequency changes. A 10 second hologram will then make a permanent record of the modal response of the test part for detailed analysis with our MODEL HV-160 Hologram Viewer.

Applications

Modal Analysis
Thermal Deformation Studies
Stress-Strain Relationships
Creep Studies
Strain Analysis of Mechanical Components
Nondestructive Evaluation

Other Required Equipment

LS-2400 Laser System or use your laser, optical components and vibration isolation table.

For more information, contact your nearest LTI representative or our factory directly.

Specifications

Control Console

Height	16 inches
Width	19 inches
Depth	21¼ inches
Weight	22 pounds
Electrical Requirements	110 VAC, 2A

Camera Unit

Height	9¾ inches
Width	12 inches
Depth	15¼ inches
Weight	18 pounds
Film	35 mm, unsprocketed LASER-TEST
Spacial Resolution	1200 Lines/mm
Exposure Sensitivity at 633nm.	8 ergs/cm²
Processing Fluid	HOLOBATH
Hologram Process Time	2 to 8 seconds

The HOLOMATIC 6000 Holographic camera is patented in the United States and abroad with additional patents pending.

Specifications subject to change without notice.

Time-average hologram showing modal patterns on a turbine blade vibrating at 10,575 hz

Holographic determination of impact damage in a composite structure

For full information, write or phone:

LASER TECHNOLOGY, INC.
1055 W. Germantown Pike, Norristown, PA 19404 • Phone 215/631-5043 • Telex 846134

END

FILMED

1-84

DTIC